이학박사 학위논문

Research on systemic regulation of neuromuscular junction maturation by fibro-adipogenic progenitor cells

근육의 섬유-지방성 전구세포에 의해 온몸에서 조절되는 신경근육접합의 성숙에 관한 연구

2022년 8월

서울대학교 대학원

생명과학부 생명과학전공

박 인 국

근육의 섬유-지방성 전구세포에 의해 온몸에서 조절되는 신경근육접합의 성숙에 관한 연구

지도 교수 공 영 윤

이 논문을 이학박사 학위논문으로 제출함

2022년 8월

서울대학교 대학원

생명과학부 생명과학전공

박 인 국

박인국의 이학박사 학위논문을 인준함

2022년 7월

위 원 장 석 영 재 (인)

부위원장 공 영 윤 (인)

위 원 정 종 경 (인)

위 원 김 종 서 (인)

위 원 김 지 훈 (인)

Abstract

Research on systemic regulation of neuromuscular junction maturation by fibro-adipogenic progenitor cells

Inkuk Park

School of Biological Sciences

Seoul National University

Skeletal muscle consists almost half of the human body which is maintained and functions by the interplay of many cells including myofibers, muscle stem cells (MuSCs), motor neurons, and fibro-adipogenic progenitors (FAPs). FAPs are muscle residential mesenchymal cells that support muscle homeostasis and regeneration upon injury by regulating myofibers and MuSCs. However, the role of FAPs in regulating other cell types in muscle tissue remains largely unknown.

Neuromuscular junction (NMJ) is a specialized synapse where the electric signal from motor neurons is transformed into a chemical signal of acetylcholine and thus induces muscle contraction. Since

synchronized and controlled signal transduction in NMJ is critical for muscular function, molecular signals such as agrin, neuregulin, and acetylcholine from neurons and terminal Schwann cells have been thoroughly investigated to be involved in the formation, maturation, and maintenance of NMJ structure and function. However, the systemic regulation and coordination of NMJ maturation and maintenance remain poorly understood.

In this study, I showed that FAPs play a pivotal role in the maturation and maintenance of NMJ and the survival of motor neurons through systemic regulation. By analyzing the effect of local transplantation of FAPs into the limb muscle tissue of the mouse model bearing dysfunctional NMJ, I revealed the local and global intervention of FAPs on NMJ development and maintenance. By investigating the transcriptome and secretome of FAPs, I identified a novel protein, granzyme E, which is specifically expressed and secreted by FAPs, that regulates the NMJ and motor neurons. This study defines a unique mechanism by which skeletal muscles establish and maintain their integrity by regulating the neuronal innervation and provides a comprehensive understanding of neuromuscular systems and their crosstalk with non-neuronal cells.

Keyword : Muscle mesenchymal cell; Fibro-adipogenic progenitor; Neuromuscular junction; Granzyme

Student Number : 2015-20431

Table of Contents

List of Figures

Background

Skeletal Muscle

Skeletal muscles consist almost half of our body and are critically required for motor functions (Frontera and Ochala, 2015). Skeletal muscles convert chemical energy stored in glucose or ATP into mechanical force to generate power, and produce movement and activity so that animals can live (Frontera and Ochala, 2015). They also play a critical role as a metabolic organs storing amino acids and carbohydrates, controlling glucose levels, generating heat to maintain body temperature, and consuming the majority of oxygen and fuel during physical activity and exercise (Frontera and Ochala, 2015).

Skeletal muscles are comprised of several types of different cells with distinct functions: myofibers, muscle stem cells (MuSCs), immune cells, endothelial cells and neighboring pericytes, motor/sensory neurons, Schwann cells and fibro-adipogenic progenitors (FAPs) (Bentzinger et al., 2013) (Fig. 1). Myofibers are syncytial cells with multiple myonuclei which are formed by accretion of myogenic progenitor cells (Relaix et al., 2021). Myofibers accomplish unique contractile functions by actin-myosin interaction in the basic cellular unit, sarcomere (Mukund and Subramaniam, 2020). MuSCs, also known as satellite cells, have robust proliferation and differentiation capacity to generate myofibers and regenerate under injured circumstances (Relaix et al., 2021). Immune cells not only play a fundamental role in tissue repair and pathogen clearance

but also control muscle homeostasis by regulating MuSCs and clearing cellular debris resulting from daily contractile function (Pillon et al., 2013; Sciorati et al., 2016). Endothelial cells and neighboring pericytes deliver the oxygen and fuels required for muscular functions and regulate vessel growth, angiogenesis, and permeability (Cappellari and Cossu, 2013). Motor and sensory neurons with Schwann cells sense postures and relay the neural signal required for voluntary movement. Due to the proportion and importance of myofibers and MuSCs in muscular function, molecular signaling and interactions controlling the functionality of MuSCs and myofibers have been thoroughly investigated while the functions of other cell types were mainly addressed in terms of MuSC regulation (Heredia et al., 2013; Joe et al., 2010; Lukjanenko et al., 2019; Saito et al., 2020; Uezumi et al., 2021).

Fig. 1. Cellular components consisting skeletal muscle. Skeletal muscle consists of myogenic cells (MuSCs, muscle fiber) and supporting cells (endothelial cell, immune cell, neuron, FAP).

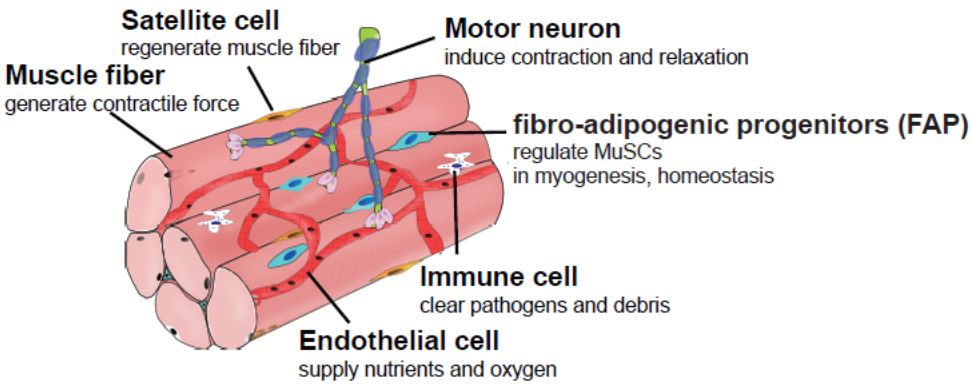
Satellite cell
regenerate muscle fiber
Muscle fiber
generate contractile force
Motor neuron
induce contraction and relaxation
fibro-adipogenic progenitors (FAP)
regulate MuSCs
in myogenesis, homeostasis
Immune cell
clear pathogens and debris
Endothelial cell
supply nutrients and oxygen

Fibro-adipogenic progenitor

Fibro-adipogenic progenitors (FAPs), are mesenchymal cells that reside between myofibers. At an early embryonic development stage, T-cell factor 4 (Tcf-4)$^{+}$ mesenchymal cells from the somatic lateral plate mesoderm migrate into the limb field and form limb buds (Kardon et al., 2003). Some of the mesenchymal cells intermingle with muscle progenitor cells, originating from abaxial dermomyotome, and develop into FAPs. FAPs themselves do not express myogenic markers (eg. Pax3, Pax7) nor fuse into myotubes, however, their Wnt-b-catenin pathway is critical for muscle prepatterning and thus myogenic differentiation in the formation of embryonic limb muscles (Kardon et al., 2003). Also, they promote slow myogenesis and switch from fetal to adult myofibers via stimulating the expression of slow and mature myosin heavy chain and the formation of large multinucleate myofibers (Mathew et al., 2011) (Fig. 2).

Along with myogenesis, they have been proposed as a critical regulator for adult muscle homeostasis and regeneration by modulating muscle microenvironments by secretion of cytokines, extracellular matrix proteins, and immuno-modulating molecules (Heredia et al., 2013; Joe et al., 2010; Lukjanenko et al., 2019; Mozzetta et al., 2013; Wosczyna et al., 2019). In homeostatic muscles, long-term depletion of FAPs results in the decrease of MuSC number and muscle mass and strength which suggests the role of FAPs in the maintenance of the MuSC population and its turnover (Uezumi et al.,

2021; Wosczyna et al., 2019). During muscle regeneration, FAPs robustly proliferate along with regenerating MuSCs to support their proper function (Lemos et al., 2015; Malecova et al., 2018). Genetic ablation of FAPs during acute injury delays muscle regeneration mainly through blockade of MuSC expansion (Wosczyna et al., 2019). In aged mice, FAPs themselves have been suggested as the major contributors to intramuscular ectopic adipocyte accumulation and fibrosis in skeletal muscles (Contreras et al., 2019; Gonzalez et al., 2017; Madaro et al., 2018; Uezumi et al., 2010, 2011, 2014). Aged FAPs also lose their capacity to support MuSC expansion following muscle injury due to altered secretion of WISP-1 (Lukjanenko et al., 2019) (Fig. 2). Recently, many studies revealed the physiological roles and pathological conditions of young and aged FAPs in terms of the development and regulation of MuSCs. However, molecular crosstalk between FAPs and other cell types consisting of muscle tissue has not been well-investigated.

With current progress in single-cell omics technologies, the transcriptional diversity and heterogeneity of PDGFRa^{+} muscle-resident FAPs have been thoroughly investigated (Giordani et al., 2019; Malecova et al., 2018; Oprescu et al., 2020; Scott et al., 2019). Two major subpopulations of FAPs have been described (FAP1 and FAP2) in undamaged muscles which have distinct molecular signatures. FAP1 primarily expresses ECM-related genes such as Col4a1, 4a2, Col6a1, 6a2, 6a3, Col15a1, Lum, Sparcl1, Podn, Smoc2, Mgp, and Bgn, whereas FAP2 subpopulation shows molecular signatures regarding multiple biological programs and cell signaling

pathways such as Sfrp4, Igfbp5, Sema3c, Dpp4, Tgfrb2, and Wnt2 (Scott et al., 2019). By the way, as previously described, FAPs are activated and robustly proliferate following muscle injury (Lemos et al., 2015; Malecova et al., 2018). During muscle regeneration, distinct subpopulations of FAPs merge into a single cluster of activated FAPs expressing chemokine genes like Cxcl5, Cxcl3, Ccl7, and Ccl2 (Oprescu et al., 2020). They progressively transform into $Wisp1^{+}$ and $Dlk1^{+}$ FAPs and eventually into resting subpopulations (Oprescu et al., 2020). A specific subpopulation of $VCAM{-}1^{+}$ FAPs transiently emerges, vastly expands, and regulates muscle regeneration which is absent in uninjured homeostatic muscles (Malecova et al., 2018) (Fig. 3). Despite the great improvement in the understanding of FAP heterogeneity, the vast majority of studies focus on the effect of FAPs on MuSCs and myofiber regulation missing the importance of interplay between other cells rather than the muscle itself.

Fig. 2. Formation and function of FAPs during myogenesis and homeostasis. Tcf−4^{+} mesenchymal cells migrate to the limb field during embryogenesis and develop into FAPs. FAPs regulate muscle prepatterning and myogenic differentiation in embryo and support myofibers in adult homeostatic muscles. FAPs are activated by muscle injury and secrete expansion signal for MuSCs to regenerate myofibers. In aged or pathological muscles, FAPs differentiate into ectopic adipocytes or fibroblasts resulting in decrease of muscle function.

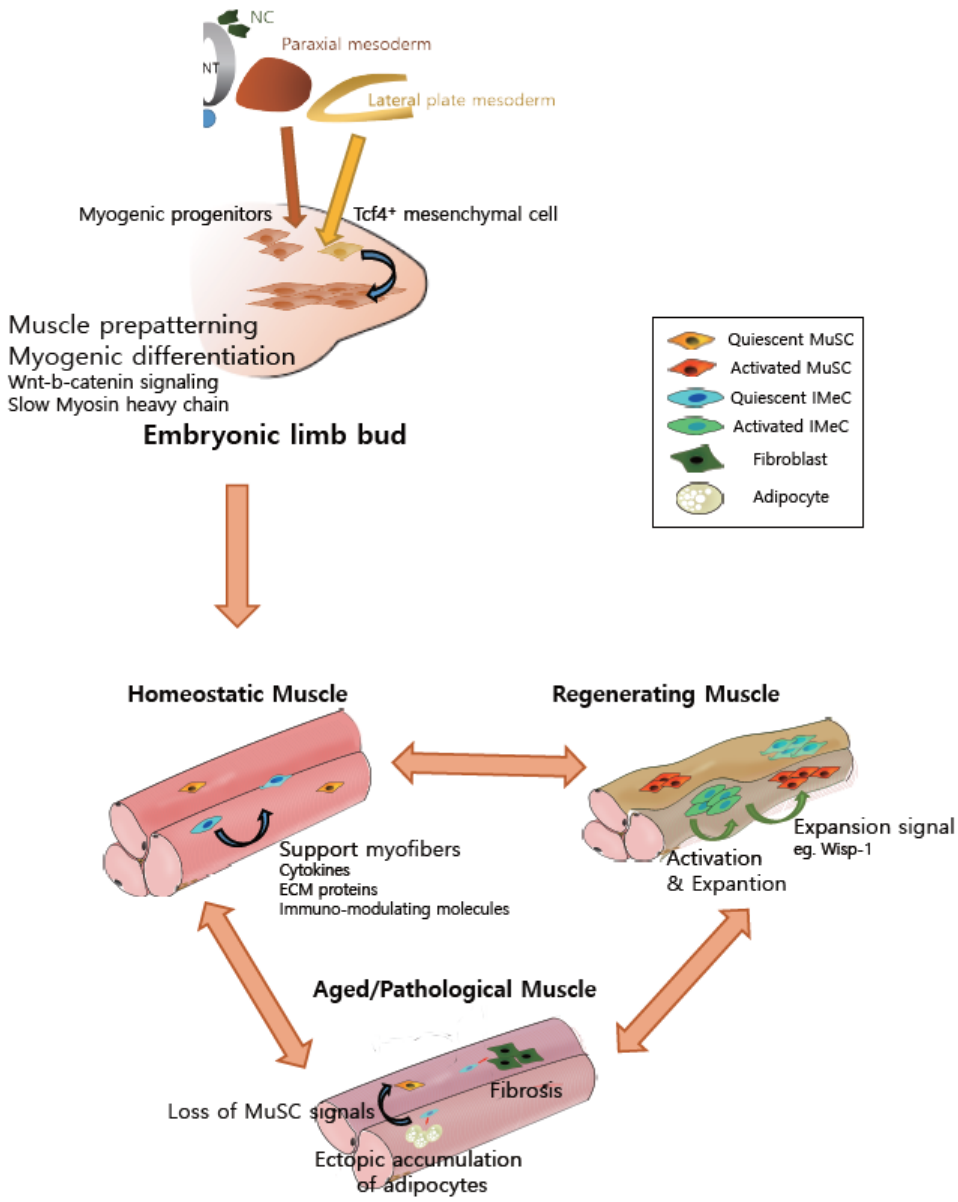
NC
Paraxial mesoderm
NT
Lateral plate mesoderm
Myogenic progenitors
Tcf4+ mesenchymal cell
Muscle prepatterning
Myogenic differentiation
Wnt-b-catenin signaling
Slow Myosin heavy chain
Embryonic limb bud
Quiescent MuSC
Activated MuSC
Quiescent IMeC
Activated IMeC
Fibroblast
Adipocyte
Homeostatic Muscle
Regenerating Muscle
Support myofibers
Cytokines
ECM proteins
Immuno-modulating molecules
Activation
& Expantion
Expansion signal
eg. Wisp-1
Aged/Pathological Muscle
Loss of MuSC signals
Fibrosis
Ectopic accumulation
of adipocytes

Fig. 3. Cellular heterogeneity of FAPs in activated and resting FAPs. In homeostatic muscles, FAPs are sub-divided into 2 subpopulations: $Cxcl14^+$ FAP1 and $Dpp4^+$ FAP2. FAP1 primarily expresses ECM-related genes, while FAP2 shows molecular signature regarding multiple biological programs and cell signaling pathways. Upon muscle injury, both subpopulations of FAPs is activated into $Vcam1^+$ FAPs which secrete chemokines facilitating muscle regeneration. Along with muscle regeneration, activated FAPs become $Wisp1^+$, $Dlk1^+$ FAPs, and finally return to FAP1 and FAP2. Despite the great improvement in the understanding of FAP heterogeneity, the vast majority of studies focus on the effect of FAPs on MuSCs and myofiber regulation missing the importance of interplay between other cells rather than the muscle itself.

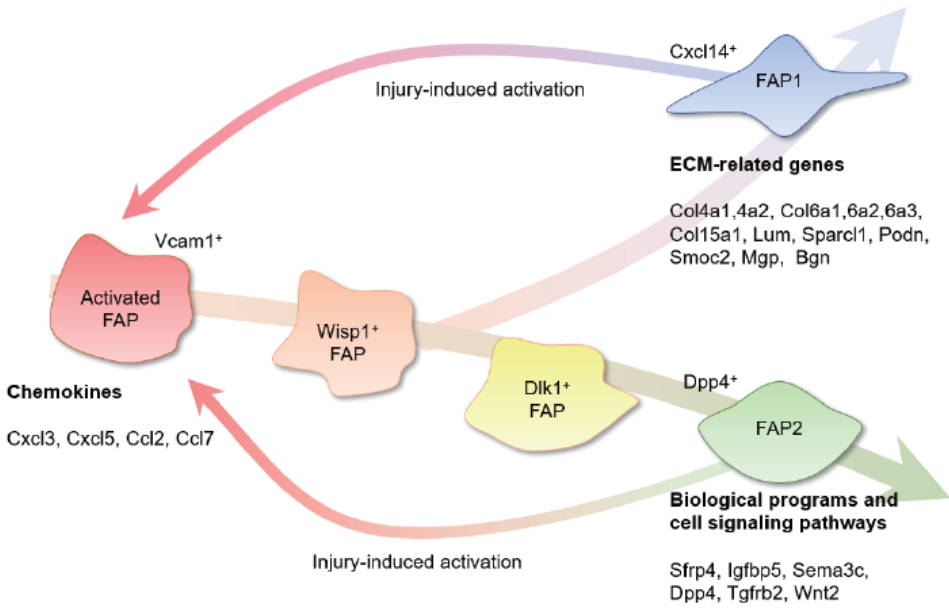
Cxcl14+
FAP1
Injury-induced activation
ECM-related genes
Col4a1,4a2, Col6a1,6a2,6a3,
Col15a1, Lum, Sparcl1, Podn,
Smoc2, Mgp, Bgn
Vcam1+
Activated
FAP
Wisp1+
FAP
Dlk1+
FAP
Dpp4+
FAP2
Chemokines
Cxcl3, Cxcl5, Ccl2, Ccl7
Biological programs and
cell signaling pathways
Sfrp4, Igfbp5, Sema3c,
Dpp4, Tgfrb2, Wnt2
Injury-induced activation

Neuromuscular junction

Neuromuscular junction (NMJ) is a highly specialized synapse formed between the motor neuron axons and skeletal muscles. It consists of a presynaptic axon terminal of the motor neuron, Schwann cells that cover and support the axon terminal, synaptic basal lamina, and postsynaptic acetylcholine receptor (AchR) clusters (Joshua R. Sanes and Jeff W. Lichtman, 2001; Wu et al., 2010) (Fig. 4A). NMJ development begins from embryos and further maturation occurs during postnatal growth. The most dramatic changes occur at the postsynaptic membrane during postnatal maturation of the NMJ: the neonatal plaque-like AChR clusters develop into multi-perforated pretzel-like structures (Shi et al., 2012) (Fig. 4B). The initial prepatterned AChR clusters are spontaneously formed at the center of muscle fibers, which is independent of the nerve terminal of motor neurons (Lin et al., 2001). Then, proteoglycan agrin released from motor neuron terminals drive postsynaptic maturation through activation of the muscle-specific kinase (MuSK) dependent and independent signaling (DeChiara et al., 1996; Gautam et al., 1996). In addition to agrin derived from nerve terminals, several factors from Schwann cells and myofibers through the reciprocal stimulation drives the maturation and maintenance of NMJ (Barik et al., 2016; Feng and Ko, 2008; Li et al., 2018; Lin et al., 2000; Remédio et al., 2016; Yang et al., 2001) (Fig. 4C).

Many studies on muscular diseases including spinal muscular atrophy (SMA) and amyotrophic lateral sclerosis (ALS) suggest the

relevance of NMJ defects on neuromuscular diseases (Harding et al., 2015; Kariya et al., 2008; Moloney et al., 2014; Pollari et al., 2014; Valsecchi et al., 2015). In SMA model mice, synaptic defects such as impaired plaque to pretzel-like transition of AChR clusters, neurofilament accumulation, poor terminal arborization, and immature endplates have been observed (Bowerman et al., 2007, 2009; Kariya et al., 2008; Kreutzer et al., 2012). These defects precede denervation and death of motor neurons, muscle weakness, and atrophy (Wyatt and Keirstead, 2010). NMJ defects are also identified in ALS at a very early stage prior to symptom onset, albeit responsible genes of ALS have not yet been demonstrated except superoxide dismutase-1 (Moloney et al., 2014).

Initial studies using SMA mouse models proposed that sufficient expression of Smn, a genetic cause of SMA phenotypes, in motor neurons would be critical for NMJ maturation (McGovern et al., 2015). However, recent studies using genetic models and AAV or ASO treatment with a complementary decoy oligonucleotide administration suggest that the enhanced SMN in motor neurons and muscle fibers is not sufficient to rescue synaptic defects of NMJ in SMA mouse models (Besse et al., 2020; Hua et al., 2011, 2015; Kariya et al., 2014) suggesting that other factors or yet unidentified cells in the peripheral tissues may play critical roles in NMJ maturation in which sufficient Smn level is required for their proper function.

Fig. 4. Neuromuscular junction (NMJ) and its regulatory signals. (A) NMJ consists of a presynaptic axon terminal of the motor neuron, Schwann cells that cover and support the axon terminal, synaptic basal lamina, and postsynaptic acetylcholine receptor (AchR) clusters. (B) During postnatal development, multi-innervated NMJs become mono-innervated NMJs and the neonatal plaque-like AChR clusters develop into multi-perforated pretzel-like structures. (C) Secretory signals from nerve termainal or Schwann cells such as agrin, acetylcholine, neuregulins play critical role in NMJ maturation and maintenance.

A

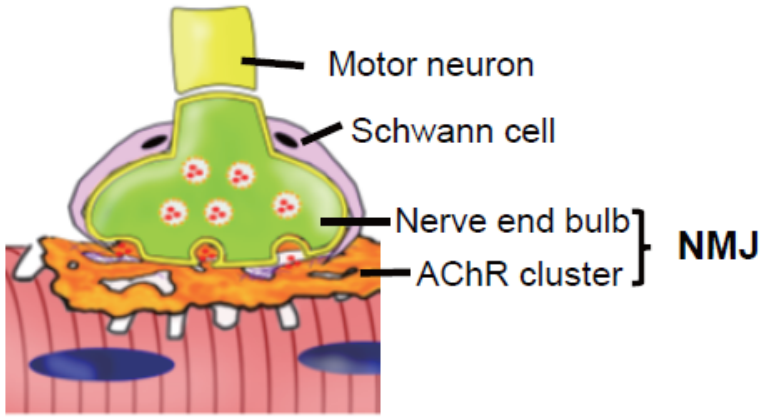
Motor neuron
Schwann cell
Nerve end bulb
AChR cluster
NMJ

B

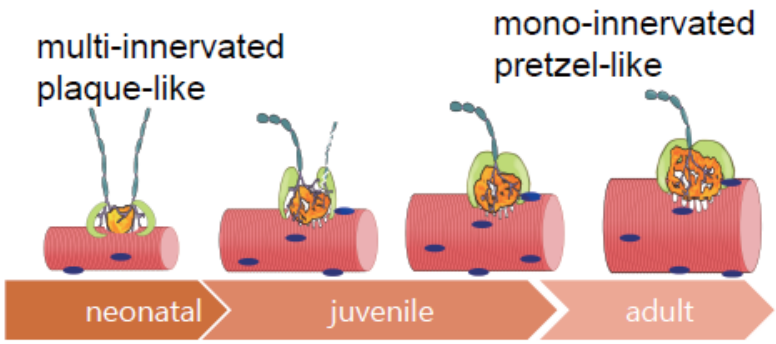
multi-innervated
plaque-like
mono-innervated
pretzel-like
neonatal
juvenile
adult

C

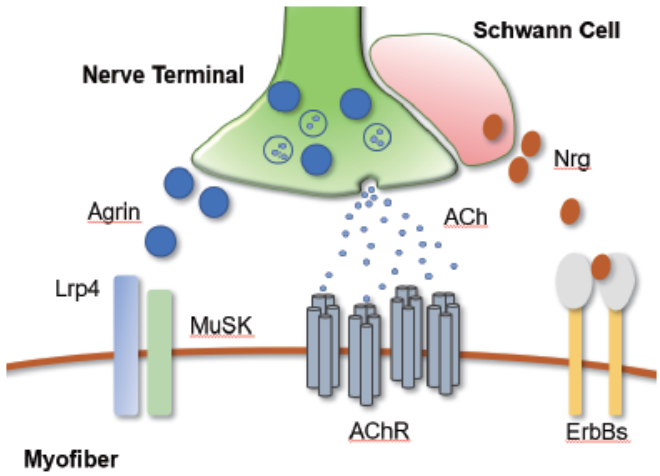
Schwann Cell
Nerve Terminal
Nrg
Agrin
ACh
Lrp4
MuSK
AChR
ErbBs
Myofiber

BRCA-associated protein 1

BRCA-associated protein 1 (Bap1), also called ubiquitin carboxy-terminal hydrolase 2 (Uchl2), is a deubiquitinating enzyme that removes ubiquitin from its protein substrate, therefore, regulating the function and stability of target proteins (Louie and Kurzrock, 2020). Bap1 was originally discovered in 1998 as a novel ubiquitin hydrolase that binds to the BRCA RING finger and enhances the tumor suppressor function of BRCA (Jensen et al., 1998). Recent studies revealed that Bap1 not only plays a pivotal role in tumor suppression but also regulates proteins involved in DNA damage repair, chromatin modulation, cell cycle control, cell death, cellular proliferation, and differentiation by altering ubiquitin signaling of its target proteins (Bononi et al., 2017; Machida et al., 2009; Nishikawa et al., 2009; Scheuermann et al., 2010; Shrestha et al., 2019; Wang et al., 2016; Zhao et al., 2017) (Fig. 5A). Given the functional role of Bap1 in cellular processes as well as tumor suppression, the mutation in the *Bap1* gene has been suggested to cause a variety of tumors (Murali et al., 2013).

Bap1 gene consists of 17 exons encoding 729 amino acids comprising ~90kDa protein. The catalytic activity for deubiquitination of Bap1 protein is a ubiquitin carboxy-terminal hydrolase (UCH) domain located in its N-terminal region (Jensen et al., 1998). Target protein for deubiquitination is recognized by other protein-binding motifs for Host Cell Factor 1 (HCF1), BRCA1, ASXL1/2, FoxK1/K2, and YY1 (Wang et al., 2016). The C-terminal

region contains two nuclear localization signals to transport Bap1 protein into the nucleus where it can regulate primary target proteins: transcription factors (Ventii et al., 2008) (Fig. 5B).

Fig. 5. The structure and function of Bap1 protein. (A) Bap1 regulates proteins involved in DNA damage repair, chromatin modulation, cell cycle control, cell death, cellular proliferation, and differentiation by altering ubiquitin signaling of its target proteins. (B) Bap1 contains ubiquitin carboxy-terminal hydrolase (UCH) domain which carries deubiquitinating activity, HCF-1-binding motif (HBM) and C-terminal domain (CTD) for target protein binding.

A

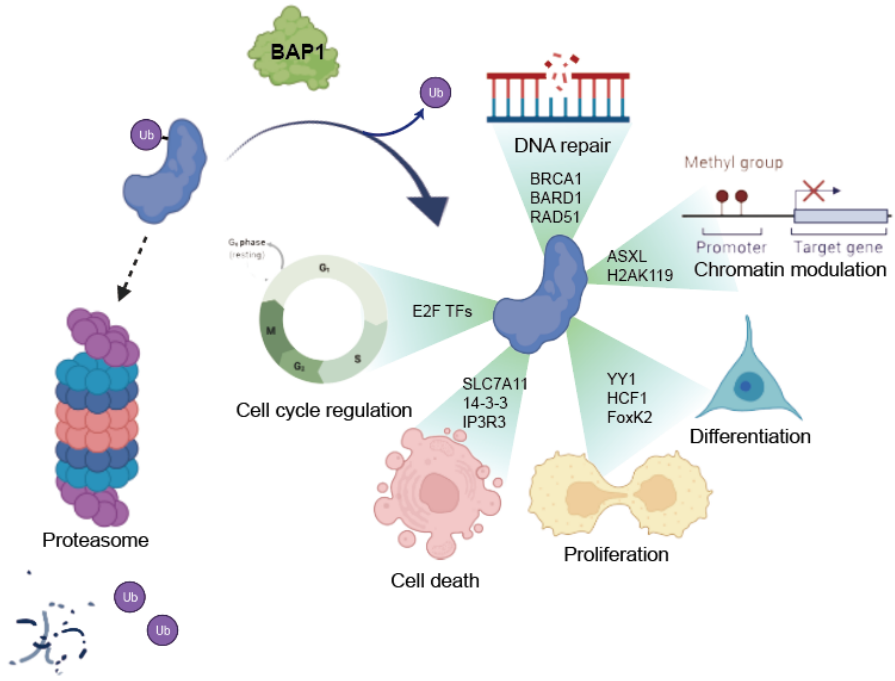
BAP1
Ub
Ub
DNA repair
BRCA1
BARD1
RAD51
Methyl group
Promoter
Target gene
Chromatin modulation
ASXL
H2AK119
E2F TFs
Cell cycle regulation
SLC7A11
14-3-3
IP3R3
YY1
HCF1
FoxK2
Differentiation
Proliferation
Cell death
Proteasome
Ub
Ub

B

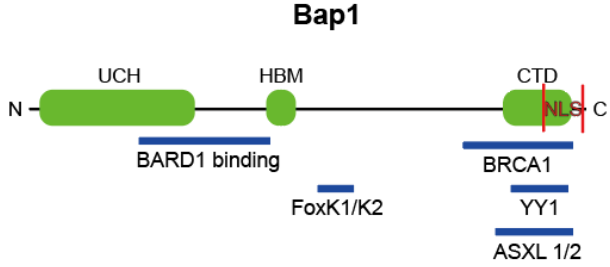
Bap1
UCH
HBM
CTD
N
NLS
C
BARD1 binding
FoxK1/K2
BRCA1
YY1
ASXL 1/2

Granzyme

Granzymes are chymotrypsin-like, structurally-related serine proteases mainly secreted from cytotoxic T lymphocytes and natural killer (NK) cells which induce target cell death. Cytotoxic T cells and NK cells secrete cytotoxic granules containing pore-forming protein perforin and granule-associated proteases to eliminate the infected or malignant cells. Granzymes are major cytotoxic granule-associated proteases that are transported into the target cell cytoplasm by perforin pores and induce caspase-dependent or -independent apoptosis (Bots and Medema, 2006; Catalfamo and Henkart, 2003) (Fig. 6).

In humans, five different granzymes have been discovered, annotated, and described for their cytotoxic functions: granzymes A, B, H, K, and M (Grossman et al., 2003) (Fig. 7A). Orthologous genes for granzymes A, B, K, and M can be found in murine genome. Granzyme C has been thought of as a murine orthologue of granzyme H (Johnson et al., 2003). Meanwhile, the murine genome encodes six additional granzymes (granzymes D, E, F, G, L, and N) with relatively unknown functions (Fig. 7B). The most extensively studied granzymes are granzyme A and B which enter the target cells through perforin-induced channels and induce apoptosis (Bots and Medema, 2006; Chowdhury et al., 2006; Martinvalet et al., 2005; Trapani and Sutton, 2003). Many studies have reported the cytotoxic functions of granzymes, including granzyme C, F, and M, in numerous combinations of target cells and contexts (Johnson et al., 2003; Kelly

et al., 2004; Shi et al., 2009). However, recent studies have demonstrated the non-cytotoxic function of granzyme proteins. Granzyme D is induced in mast cells during bacterial infection or allergic conditions (Rönnberg et al., 2013). Granzyme G is expressed in a 2-cell stage embryo and is required for the maternal-zygotic transition (Tsai et al., 2010). These reports suggest that further studies on individual granzymes are essential for an in-depth understanding of their non-cytotoxic functions.

Fig. 6. Canonical cytotoxic function of granzyme protease. Cytotoxic T lymphocytes and natural killer (NK) cells secrete pore-forming protein perforin and granzymes which then transported into target cell and induce cell death by caspase-dependent and -independent pathways.

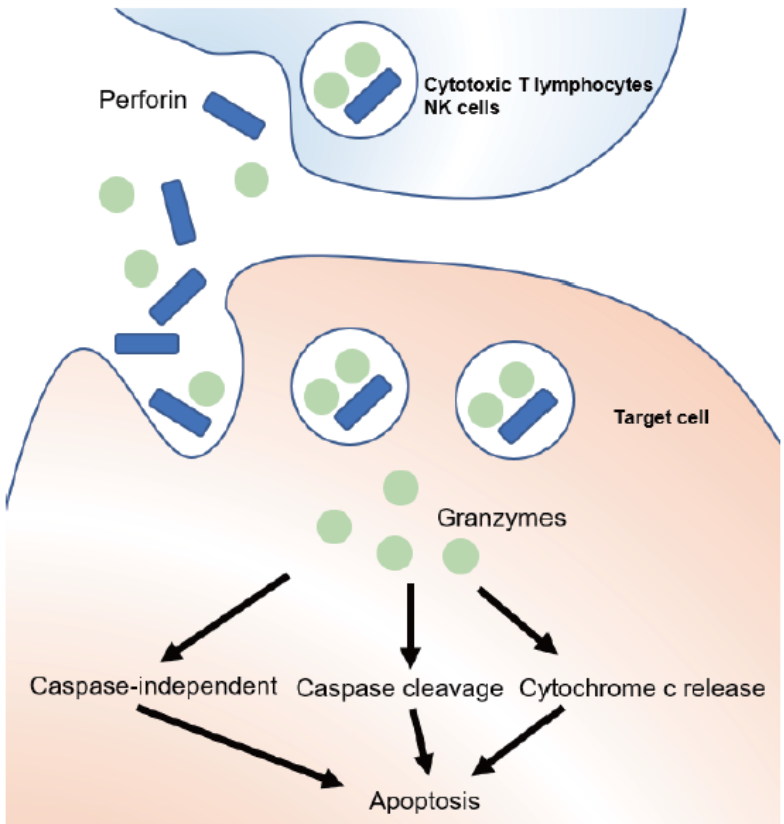
Perforin
Cytotoxic T lymphocytes
NK cells
Target cell
Granzymes
Caspase-independent
Caspase cleavage
Cytochrome c release
Apoptosis

Fig. 7. Proteins in granzyme family and their molecular phylogenetic tree. (A) In humans, granzymes A, B, H, K, and M have been discovered, annotated and described for their cytotoxic functions. (B) In mouse genome, 11 granzymes (A, B, C, D, E, F, G, K, L, M, N) have been identified.

A

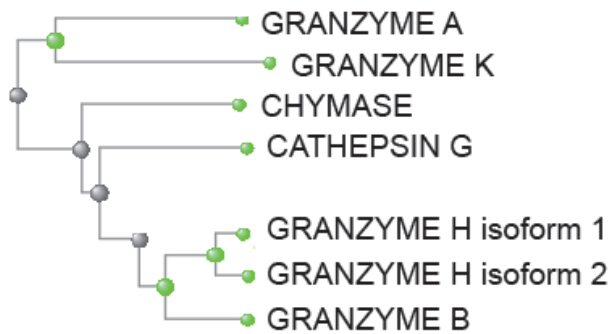
GRANZYME A
GRANZYME K
CHYMASE
CATHEPSIN G
GRANZYME H isoform 1
GRANZYME H isoform 2
GRANZYME B

B

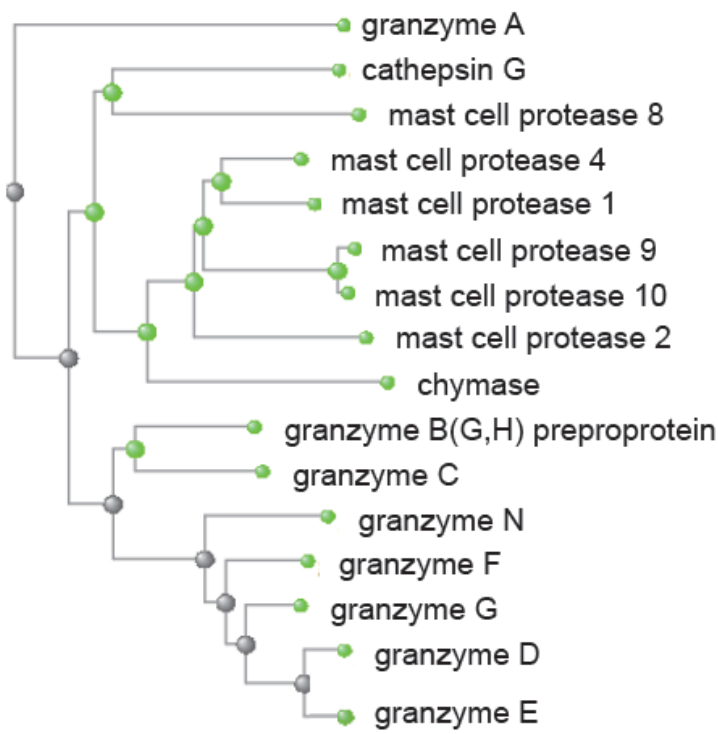
granzyme A
cathepsin G
mast cell protease 8
mast cell protease 4
mast cell protease 1
mast cell protease 9
mast cell protease 10
mast cell protease 2
chymase
granzyme B(G,H) preproprotein
granzyme C
granzyme N
granzyme F
granzyme G
granzyme D
granzyme E

Introduction

Neuromuscular junction (NMJ) is a highly specialized synapse formed between motor neurons and skeletal muscle fibers. The NMJ consists of the presynaptic axon terminal of a motor neuron, postsynaptic acetylcholine receptor (AChR) cluster, and terminal Schwann cells (Joshua R. Sanes and Jeff W. Lichtman, 2001; Wu et al., 2010). Electrical signals from motor neurons release acetylcholine in the axon terminal and activate the acetylcholine receptor, inducing muscle contraction. Synchronized and fully functional signal transduction requires postnatal maturation of the NMJ, which includes the development of neonatal plaque-like AChR clusters to pretzel-like structures (Shi et al., 2012). Several paracrine factors from motor neurons, Schwann cells, and muscle fibers, such as neural agrin, neuregulins, and glial cell-derived neurotrophic factor (GDNF), have been suggested to drive the maturation and maintenance of NMJ (Schmidt et al., 2011; Stanga et al., 2021; Tezuka et al., 2014). However, the systemic regulation and coordination of NMJ maturation and maintenance remain poorly understood.

Muscle fibro-adipogenic progenitors (FAPs) are mesenchymal cells originating from the lateral plate mesoderm. The cytokines, extracellular matrix proteins, and immune-modulators secreted by FAPs modulate the muscle microenvironment and are critical to adult muscle homeostasis and regeneration (Lemos et al., 2015; Malecova

et al., 2018; Uezumi et al., 2021; Wosczyna et al., 2019). The proliferation and expansion of the FAP population occur upon neuromuscular perturbation caused by mechanical denervation, toxin-induced injury, or neurodegenerative disorders such as amyotrophic lateral sclerosis (ALS) (Gonzalez et al., 2017; Madaro et al., 2018; Theret et al., 2021). Previously, the absolute requirement of FAPs in NMJ maturation has been suggested by analyzing the neuromuscular phenotypes in *Prrx1*^{Cre}*;Bap1*$^{f/f}$ mice and their prevention by WT FAPs (Kim et al., 2022). FAP-specific deletion of deubiquitinating enzyme Bap1 causes dysregulation of Smn protein which is critical for proper mRNA splicing (Kim et al., 2022).

In this study, I focused on how FAPs regulate NMJ maturation. FAPs are commonly observed in perimysium and epimysium rather than endomysium, particularly in perivascular space (Uezumi et al., 2010), while no specific sign of positional relevance between FAPs and NMJs has been reported. Therefore, I speculated that the regulation of NMJ maturation by FAPs needs secretory molecules transferring the signals from FAPs to the components consisting of NMJ. I revealed the critical factors for NMJ maturation are secreted from FAPs and travel through the whole body to regulate global NMJs altogether. Then, the molecular sentinel for NMJ maturation produced by FAPs was further specified as a novel protein, granzyme E, by transcriptomic and secretomic analyzes. In this study, I described, for the first time, the systemic regulation of the NMJs and the involvement of granzyme E secreted by FAPs in neuromuscular

system maturation and maintenance.

Results

Systemic regulation of neuronal innervation by FAPs

Neuromuscular defects were previously reported in *Prrx1*^{Cre}*; Bap1*$^{f/f}$ (hereafter, cKO) mice, wherein *Bap1* is specifically ablated in cells originating from the lateral plate mesoderm, including FAPs (Kim et al., 2022). However, the mechanisms through which FAPs regulate neuronal innervation of skeletal muscles remain unknown. To investigate the regulation of NMJ innervation by FAPs, I transplanted TurboGFP^{+} wild-type (WT) FAPs into the tibialis anterior (TA) and *gastrocnemius* (GA) muscles of the cKO right hindlimb and examined the NMJ in the transplanted TA, nearby *extensor digitorum longus* (EDL), contralateral TA, GA in the hindlimb, *extensor carpi radialis*, *flexor carpi radialis* and *triceps branchii* (Triceps) muscles in the forelimb (Fig. 8). Unexpectedly, local transplantation of WT FAPs rescued NMJ innervation (Fig. 9A-C) and motor endplate area (Fig. 9D) in all muscles examined, including the transplanted, contralateral hindlimb, and forelimb muscles.

To examine whether the rescue of remote NMJs was due to the migration of transplanted TurboGFP^{+} FAPs into remote muscles, the absence/presence of TurboGFP-labeled cells in each muscle was confirmed by an immunohistochemical (IHC) analysis. The transplanted TurboGFP^{+} FAPs were found only in the transplanted right TA and GA muscles but not in any other muscle, indicating systemic regulation of NMJs by transplanted FAPs (Fig. 10).

Subsequently, I performed electromyogram and behavioral tests to investigate whether the transplantation of WT FAPs into the right TA and GA muscles of cKO mice leads to functional rescues. As expected, impaired compound muscle action potential (CMAP) in cKO mice was rescued in both transplanted and contralateral GA muscles (Fig. 11). Similarly, the tail suspension test demonstrated that hindlimb posture in both legs (Fig. 12A) and the number of hindlimb swings (Fig. 12B) were rescued by local FAP transplantation. These results suggest that FAPs systemically regulate neuronal innervation in skeletal muscles.

Fig. 8. Schematic of local FAP transplantation. TurboGFP^{+} FAPs were transplanted into the right tibialis anterior (TA) and gastrocnemius (GA) muscles. Transplanted muscles [FAP(+)], contralateral muscles, and forelimb muscles [FAP(−)] of FAP−transplanted cKO mice were analyzed according to the indicated timelines.

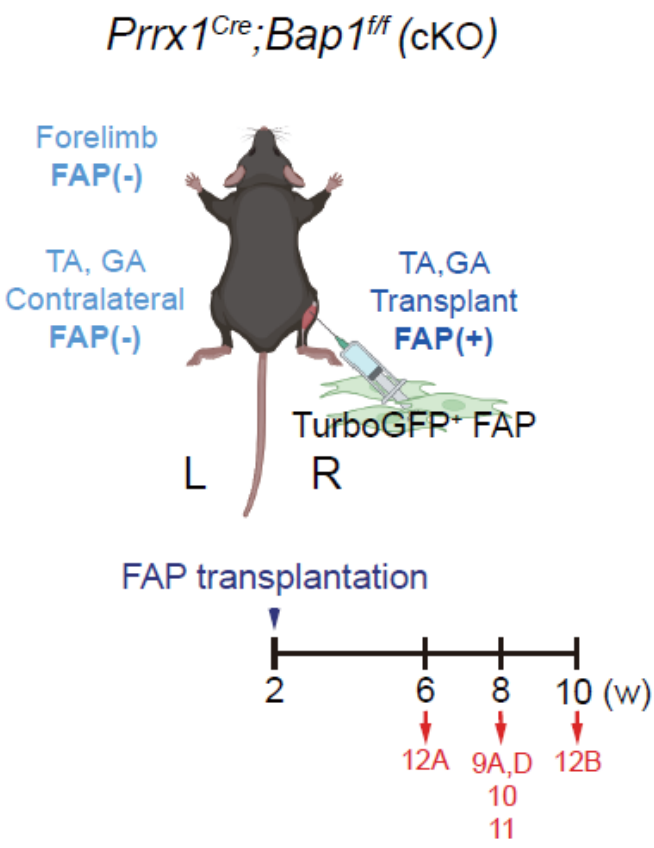
Prrx1Cre;Bap1f/f (cKO)
Forelimb
FAP(-)
TA, GA
Contralateral
FAP(-)
TA,GA
Transplant
FAP(+)
TurboGFP+ FAP
L
R
FAP transplantation
2
6
8
10 (w)
12A
9A,D
10
11
12B

Fig. 9. neuromuscular defects in cKO mice is systemically rescued by local FAP transplantation. (A) Confocal images of bungarotoxin (BTX) and neurofilaments on the TA and forelimb (*triceps branchii* or *flexor carpi radialis*) muscles. (B–C), Confocal images of bungarotoxin (BTX) and neurofilaments in the (B) *tibialis anterior* (TA) and (C) forelimb (Triceps or Flexor) muscles from WT, cKO, and FAP–transplanted cKO mice. FAP(+) and FAP(–) indicate the transplanted and contralateral/forelimb muscles, respectively. (D) Quantification of the motor endplate area of *extensor digitorum longus* (EDL) muscles from WT and cKO mice with or without FAP transplantation normalized to WT mice. WT (black), cKO (white), FAP–transplanted (blue), and contralateral (cyan) EDL of FAP–transplanted cKO mice were analyzed. Scales, 20 μm (A), 50 μm (B and C). n = 6 (D) muscles per group. One–way ANOVA followed by Tukey's pairwise comparison post hoc test (D). Data are presented as mean ± s.e.m.; *p<0.05, **p<0.01; ns, not significant.

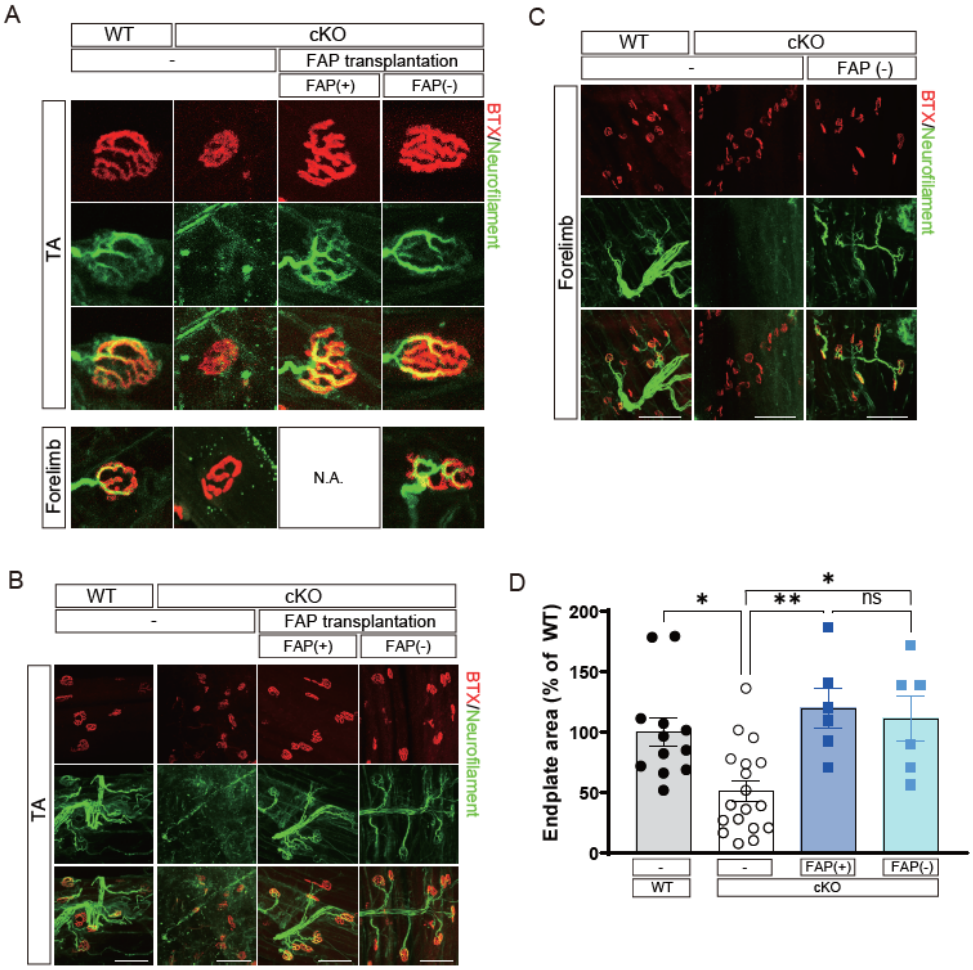
A
WT
cKO
-
FAP transplantation
FAP(+)
FAP(-)
TA
Forelimb
N.A.
BTX/Neurofilament
C
WT
cKO
-
FAP (-)
Forelimb
BTX/Neurofilament
B
WT
cKO
-
FAP transplantation
FAP(+)
FAP(-)
TA
BTX/Neurofilament
D
Endplate area (% of WT)
200
150
100
50
0
*
**
ns
*
-
-
FAP(+)
FAP(-)
WT
cKO

Fig. 10. Transplanted TurboGFP^{+} cells are found only in the transplanted muscles. Immunohistochemical images of laminin and TurboGFP staining in transplanted [FAP(+)], contralateral [FAP(−)] TA, and Triceps [FAP(−)] of FAP−transplanted cKO mice. Scale, 50 μm.

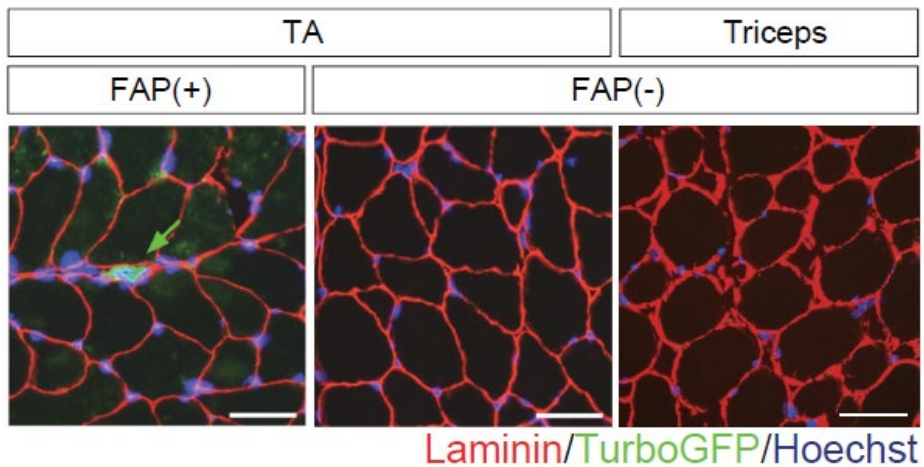
TA
Triceps
FAP(+)
FAP(-)
Laminin/TurboGFP/Hoechst

Fig. 11. Impaired compound muscle action potential (CMAP) in cKO mice is rescued in both transplanted and contralateral GA muscles. Compound muscle action potential (CMAP) amplitude measured from GA of the indicated muscles. n = 3 animals per group. One-way ANOVA followed by Tukey's pairwise comparison post hoc test. Data are presented as mean ± s.e.m.; *p<0.05; ns, not significant.

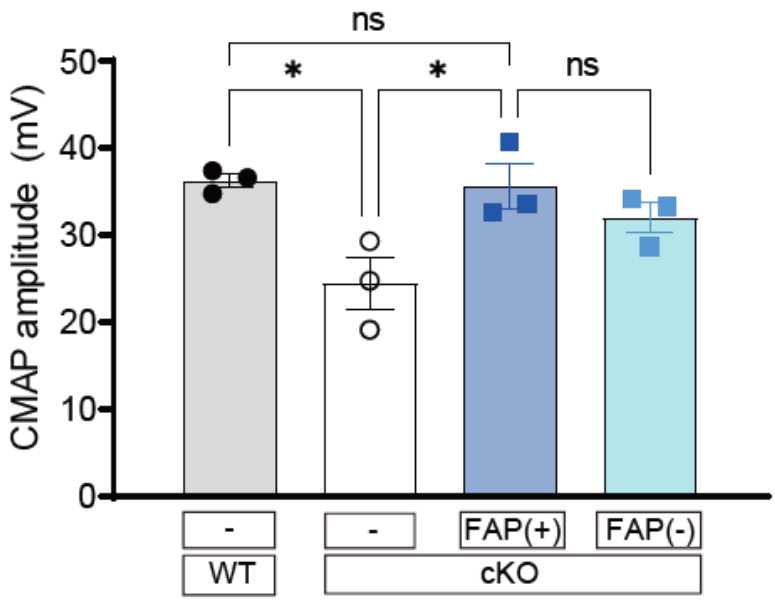
ns
*
*
ns
50
40
30
20
10
0
CMAP amplitude (mV)
-
-
FAP(+)
FAP(-)
WT
cKO

Fig. 12. Local FAP transplantation rescue the behavioral defects in cKO. (A) Hindlimb postures of WT, cKO, and FAP-transplanted cKO (cKO+FAP) mice in tail suspension test. (B) Quantification of hindlimb swings during 5 min of the tail suspension test of the indicated mice. n = 4 animals per group. Welch's ANOVA followed by Games-Howell post hoc test (B).; Data are presented as mean ± s.e.m.; ****p<0.0001; ns, not significant.

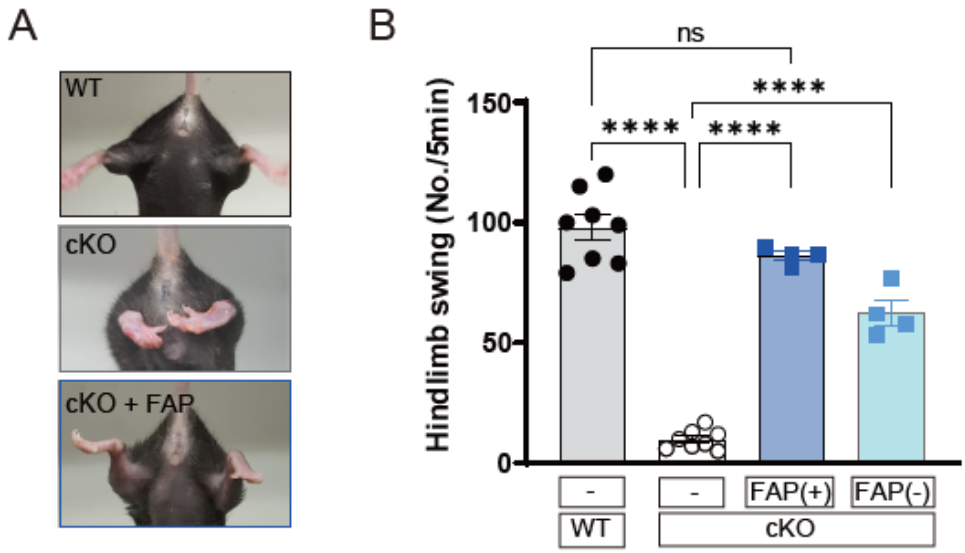
A
WT
cKO
cKO + FAP
B
ns
****
****
****
Hindlimb swing (No./5min)
150
100
50
0
-
-
FAP(+)
FAP(-)
WT
cKO

FAP-media rescue neuromuscular defects

As FAPs systemically regulate the neuromuscular system, I speculated that FAPs might secrete certain molecules that control the neuromuscular system in remote muscles. To investigate this, FAPs were isolated from *Rosa*^{CreER}; *Bap1*$^{f/f}$ mice, cultured with or without 4-hydroxytamoxifen (4-OHT) to collect FAP-conditioned media (CM) in vitro, and tested for their effects on the neuromuscular system (Fig. 13). Consequent deletion of the *Bap1* gene upon 4-OHT treatment was confirmed by quantitative reverse transcription polymerase chain reaction (qRT-PCR) (Fig. 14). The CM of WT and ⊿Bap1 FAPs were collected in serum-free α-minimum essential medium (αMEM) and packaged into poly (lactic-co-glycolic acid) (PLGA) microparticles for extended-release *in vivo* (Kang et al., 2019). I administered the microparticles every week to cKO mice and investigated whether neuromuscular defects were rescued. Notably, the administration of WT FAP-CM to cKO mice was sufficient to rescue neuromuscular defects, including abnormal hindlimb clasping, decreased CMAP amplitude, AChR endplate size, and the denervation status (Fig. 15A-G). In contrast, the injection of ⊿bap1 FAP CM did not ameliorate the neuromuscular phenotypes observed in cKO mice (Fig. 15A-G). These results suggest that FAPs regulate neuromuscular function by secreting specific factors required for NMJ maturation and function.

Fig. 13. Schematics for conditioned media (CM) collection and treatment of cKO mice. FAPs were isolated from *Rosa*^{CreER};*Bap1*$^{f/f}$ mice and cultured with the vehicle (ethanol, EtOH) or 4-hydroxytamoxifen (4-OHT). Conditioned media was encapsulated into PLGA microparticles and subcutaneously injected into cKO mice every week. Functional and histological analyses were performed according to the indicated timelines.

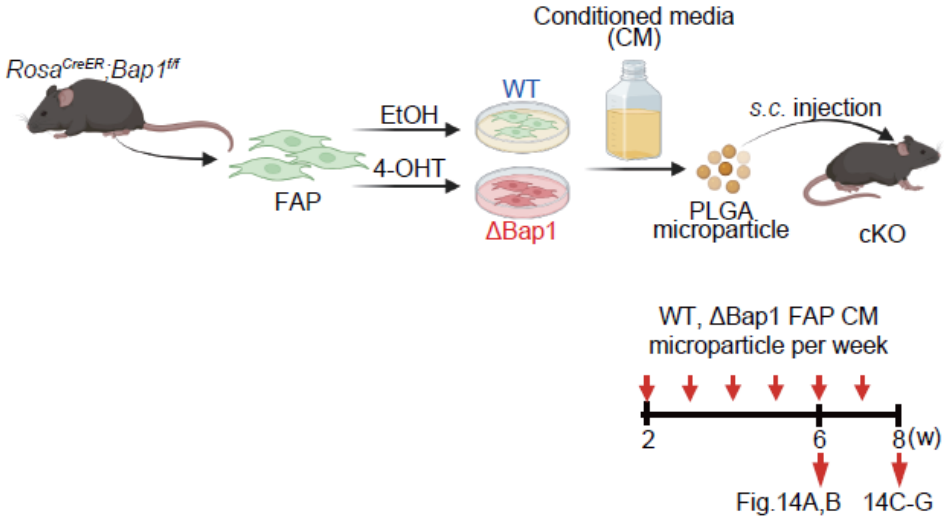
Rosa^CreER:Bap1^f/f
FAP
EtOH
4-OHT
WT
ΔBap1
Conditioned media
(CM)
PLGA
microparticle
s.c. injection
cKO
WT, ΔBap1 FAP CM
microparticle per week
2
6
8(w)
Fig.14A,B
14C-G

Fig. 14. Sufficient deletion of Bap1 upon 4-hydroxytamoxifen (4-OHT) treatment. Relative *Bap1 mRNA* expression level in $Rosa^{CreER};Bap1^{f/f}$ FAPs with or without 4-OHT treatment. n = 3 biological replicates per group. mean ± s.e.m.; Student's t-test assuming a two-tailed distribution; ****<0.0001.

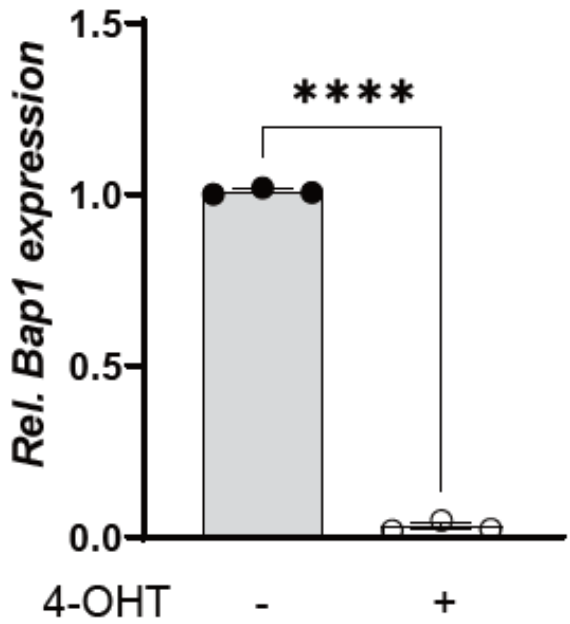
1.5
1.0
0.5
0.0
Rel. Bap1 expression
****
4-OHT
-
+

Fig. 15. Rescue of neuromuscular defects in cKO mice by conditioned media from FAPs. WT, ⊿Bap1 CM-treated cKO, and WT FAP-CM-treated cKO are indicated in black, red, and blue, respectively. (A, B), Representative images of the tail suspension test of WT and cKO mice treated with WT or ⊿Bap1 FAP-CM (A) and quantification of abnormal hindlimb clasping time during 3 min recording (B). (C, D), Representative CMAP response (C) and quantification of CMAP amplitude of GA muscles (D) from the indicated mice. (E) Confocal images of bungarotoxin (BTX) and neurofilaments on the EDL muscles of the indicated mice. (F, G) Quantification of the area occupied by acetylcholine receptor (AChR) staining (F) and degree of innervation of EDL muscles (G) from the indicated mice. Scales, 1 cm (A) and 20 μm (E). n = 3 (WT of B, D, F and G) and n = 5 (cKO, WT or ⊿Bap1 CM-treated cKO of B) animals per group. Each dot represents an individual animal or a muscle; One-way ANOVA followed by Tukey's pairwise comparison post hoc test (D). Kruskal-Wallis test followed by Dunn's post hoc test (B and F). Two-way ANOVA followed by Tukey's pairwise comparison post hoc test (G).; Data are presented as mean ± s.e.m.; *$p<0.05$, **$p<0.01$; ns, not significant.

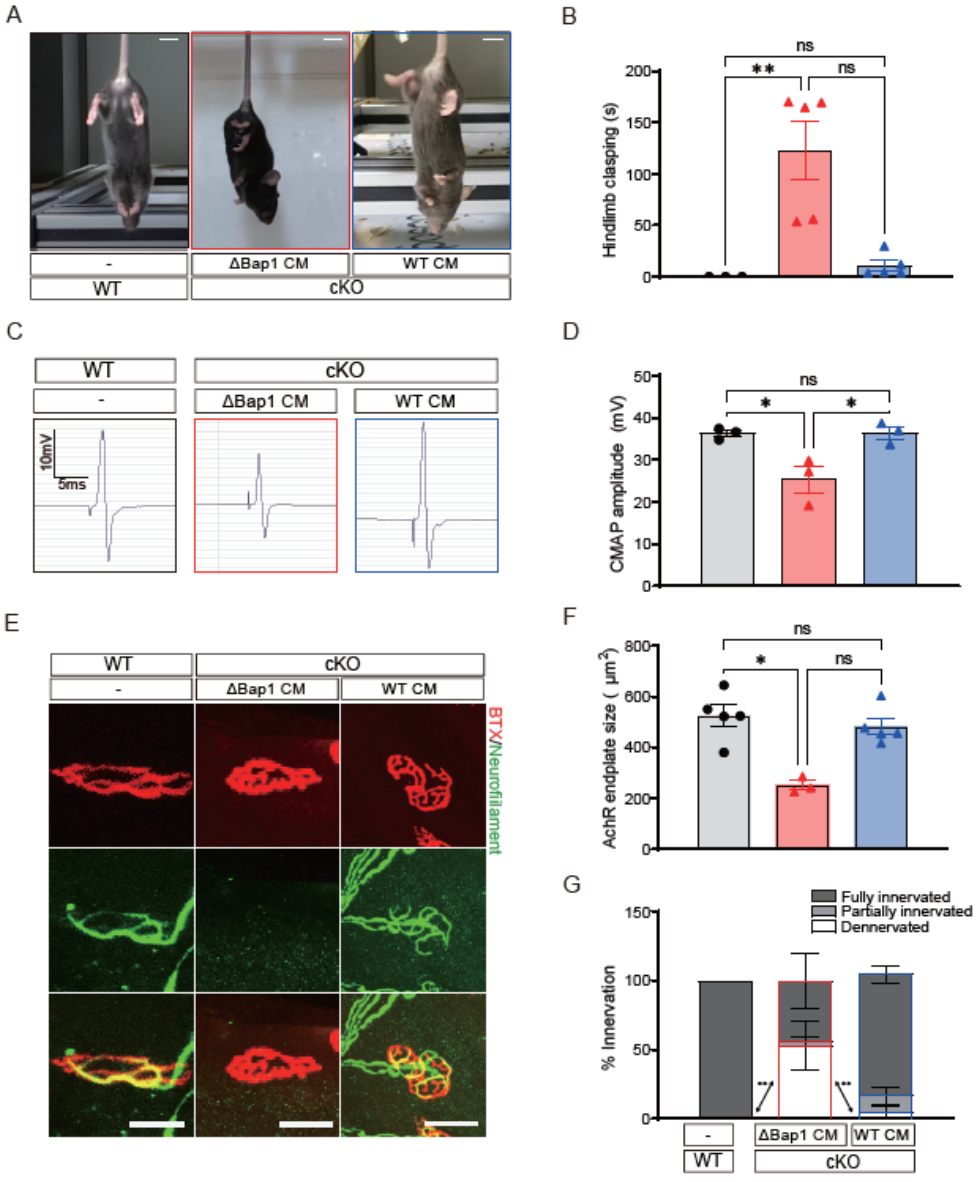
A
-
ΔBap1 CM
WT CM
WT
cKO
B
ns
**
ns
Hindlimb clasping (s)
200
150
100
50
0
C
WT
cKO
-
ΔBap1 CM
WT CM
10mV
5ms
D
ns
*
*
CMAP amplitude (mV)
50
40
30
20
10
0
E
WT
cKO
-
ΔBap1 CM
WT CM
BTX/Neurofilament
F
ns
*
ns
AchR endplate size (μm²)
800
600
400
200
0
G
Fully innervated
Partially innervated
Dennervated
% Innervation
150
100
50
0
-
ΔBap1 CM
WT CM
WT
cKO

Secretion of granzyme E by FAPs

In a previous study, it was described that the neuromuscular phenotypes observed in cKO mice were due to decreased levels of Smn in the FAPs (Kim et al., 2022). Thus, restoring functional Smn levels by overexpressing mutant forms of human SMN (SMN^{K186R}) resistant to ubiquitination and consequent degradation was sufficient to restore the functionality of ⊿Bap1 FAPs during NMJ maturation and maintenance (Kim et al., 2022). This implies that the secretory molecule responsible for NMJ maturation is under the control of the Bap1−Smn axis and that SMN^{K186R} overexpression in Bap1−null FAP is sufficient to reinstate the expression of the factor required for proper neuromuscular function. Therefore, I hypothesized that the expression and secretion of neuromuscular factors in FAPs are downregulated in response to Bap1 disruption and can be restored by overexpressing ubiquitination−resistant SMN^{K186R}. To identify candidate factors, transcriptome and secretome of WT, ⊿Bap1, and SMN^{K186R}−overexpressing ⊿Bap1 FAPs were analyzed (Fig. 16A, B). RNA sequencing analyses revealed that 1078 genes were upregulated in WT FAPs compared to ⊿Bap1 FAPs (Fig. 17). As the overexpression of SMN^{K186R}, but not SMN^{WT}, rescued the neuromuscular modulating function of ⊿Bap1 FAPs, I compared SMN^{WT} with SMN^{K186R}−overexpressing ⊿Bap1 FAPs. Briefly, 223 genes were upregulated by SMN^{K186R} overexpression compared with SMN^{WT} overexpression in ⊿Bap1 FAPs (Fig. 17). Thirty−six genes

satisfied both criteria mentioned above at the transcriptional level (Fig. 17).

To directly compare the proteins secreted by WT and ⊿Bap1 FAPs, I analyzed the secretome of cultured FAPs using the SEC61B-TurboID biotin labeling technique (Fig. 16B) (Kim et al., 2021). As canonical secretory proteins are translated and transported through the ER-Golgi pathway, most secretory proteins produced from SEC61B-TurboID transduced cells are labeled with biotin (Kim et al., 2021). Therefore, by enriching biotinylated proteins, I could observe the genuine features of the WT and ⊿Bap1 FAP secretomes. A total of 263 proteins were detected as biotinylated proteins in WT and ⊿Bap1 FAP-CM, and 20 proteins were downregulated in ⊿Bap1 FAP-CM compared with those in WT FAP-CM (Fig. 17, 18A, B).

To estimate the molecular size of the effective proteins produced by FAPs, protein fractionation was conducted by size exclusion chromatography of WT FAP-CM, and subsequent phenotypic rescue analysis was studied in cKO mice. Neuromuscular defects were rescued in cKO mice treated with the third fraction, containing protein sizes of 25-100 kDa (Fig. 19A-D). Then, I compared the transcriptome and secretome analyses of the WT, ⊿Bap1, and SMN-overexpressing FAPs. The results showed that a single gene, *granzyme E*, satisfied the changes in transcriptome and secretome levels and the protein size range (Fig. 20). The downregulation of *granzyme E* and its restoration by SMN^{K186R} overexpression were confirmed by qRT-PCR of RNA from cultured ⊿Bap1 FAPs (Fig. 21). These data suggest that granzyme E is produced and secreted

by FAPs under the control of the Bap1-Smn axis and could be the protein essential for the systemic regulation of NMJ.

Fig. 16. Schematic of transcriptome and secretome analyzes of WT, ⊿ Bap1, and SMN^{K186R}-overexpressing ⊿ Bap1 FAPs. (A) Experimental scheme of transcriptomic analysis of WT, ⊿Bap1, SMN^{WT}, or SMN^{K186R}-overexpressing ⊿Bap1 FAPs. FAPs isolated from $Rosa^{CreER};Bap1^{f/f}$ mice were cultured with vehicle (EtOH) or 4-hydroxytamoxifen (4-OHT), and RNA was collected from WT and ⊿Bap1 samples. FAPs were transduced with lentiviruses containing SMN^{WT} or SMN^{K186R} (ubiquitination-resistant SMN) and subsequently treated with 4-OHT for ⊿Bap1+SMN^{WT} and ⊿Bap1+SMN^{K186R} RNA samples. (B) Experimental scheme for secretome analysis of WT and ⊿Bap1 FAPs. FAPs isolated from $Rosa^{CreER};Bap1^{f/f}$ mice were transduced with lentivirus containing SEC61B-TurboID and treated with vehicle (EtOH) or 4-OHT, and WT and ⊿Bap1 FAP-CMs were collected for mass spectrometric analysis.

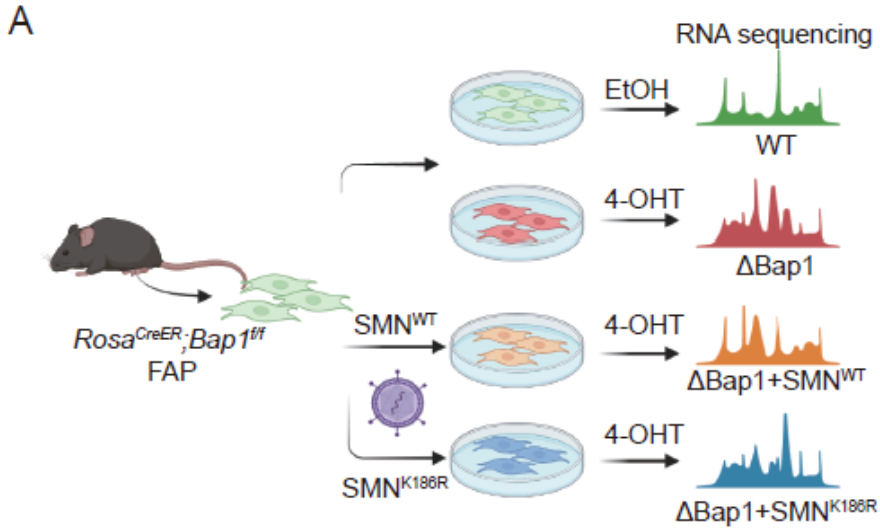
A
RNA sequencing
EtOH
WT
4-OHT
ΔBap1
Rosa^CreER;Bap1^f/f
FAP
SMN^WT
4-OHT
ΔBap1+SMN^WT
SMN^K186R
4-OHT
ΔBap1+SMN^K186R

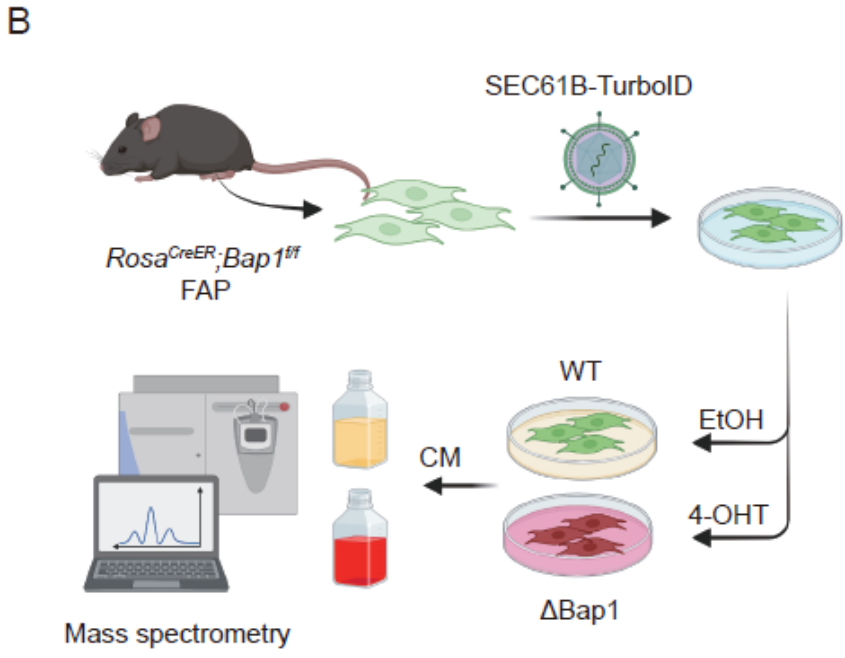
B
SEC61B-TurboID
Rosa^CreER;Bap1^f/f
FAP
WT
EtOH
CM
4-OHT
ΔBap1
Mass spectrometry

Fig. 17. Flow chart of transcriptomic and secretomic analyses. The number in brackets represent the number of genes that satisfy the criteria.

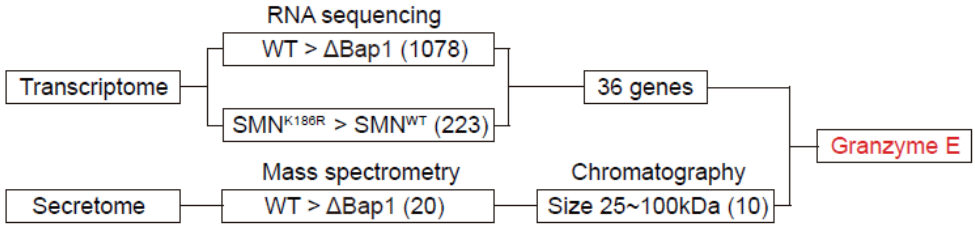
RNA sequencing
WT > ΔBap1 (1078)
Transcriptome
SMNK186R > SMNWT (223)
36 genes
Granzyme E
Mass spectrometry
Chromatography
Secretome
WT > ΔBap1 (20)
Size 25~100kDa (10)

Fig. 18. Secretome analyzes revealed distinct clusters of secreted proteins in WT and ⊿Bap1 FAP-CM. (A) Scatterplot analysis of the identified biotinylated proteins across the biological replicates. The Pearson's correlation is noted in blue. (B) Hierarchical clustering Heatmap analysis of biotinylated proteins (pre-processed with K-means clustering, K=4). The line graph depicts the abundance patterns of identified biotinylated proteins in each cluster.

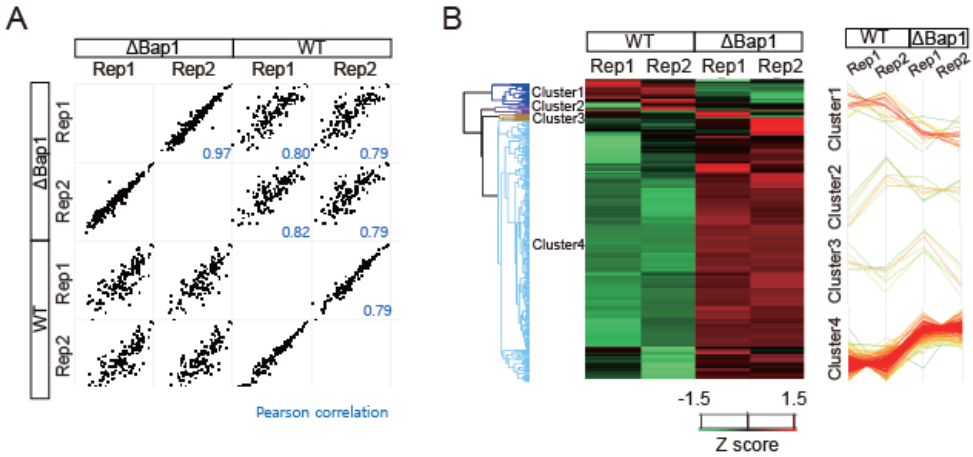
A
ΔBap1
WT
Rep1
Rep2
Rep1
Rep2
ΔBap1
WT
Rep1
Rep2
Rep1
Rep2
0.97
0.80
0.79
0.82
0.79
0.79
Pearson correlation
B
WT
ΔBap1
Rep1
Rep2
Rep1
Rep2
Cluster1
Cluster2
Cluster3
Cluster4
-1.5
1.5
Z score
WT
ΔBap1
Rep1
Rep2
Rep1
Rep2
Cluster1
Cluster2
Cluster3
Cluster4

Fig. 19. Size exclusion chromatography of WT FAP-CM showed the fraction #3 (25-100kDa) contains the NMJ maturation factor. (A) UV absorbance chromatogram and elution scheme for size-exclusion chromatography of FAP-conditioned media (CM). (B) Coomassie staining of elution fractions #3-7 from (A). (C) Compound muscle action potential (CMAP) amplitude for *gastrocnemius* (GA) muscles of cKO mice treated with elution fractions of FAP CM. Each fraction was encapsulated in PLGA microparticles and subcutaneously injected into cKO mice every week. CMAP was quantified at eight weeks. (D) Confocal images of BTX and neurofilaments of cKO and elution fraction #3- or 4-treated cKO mice. Scales, 20 μm (D). n = 3 muscles per group (C). One-way ANOVA followed by Tukey's pairwise comparison post hoc test (C). Data are presented as mean ± s.e.m.; *p<0.05, **p<0.01, ***p<0.001.

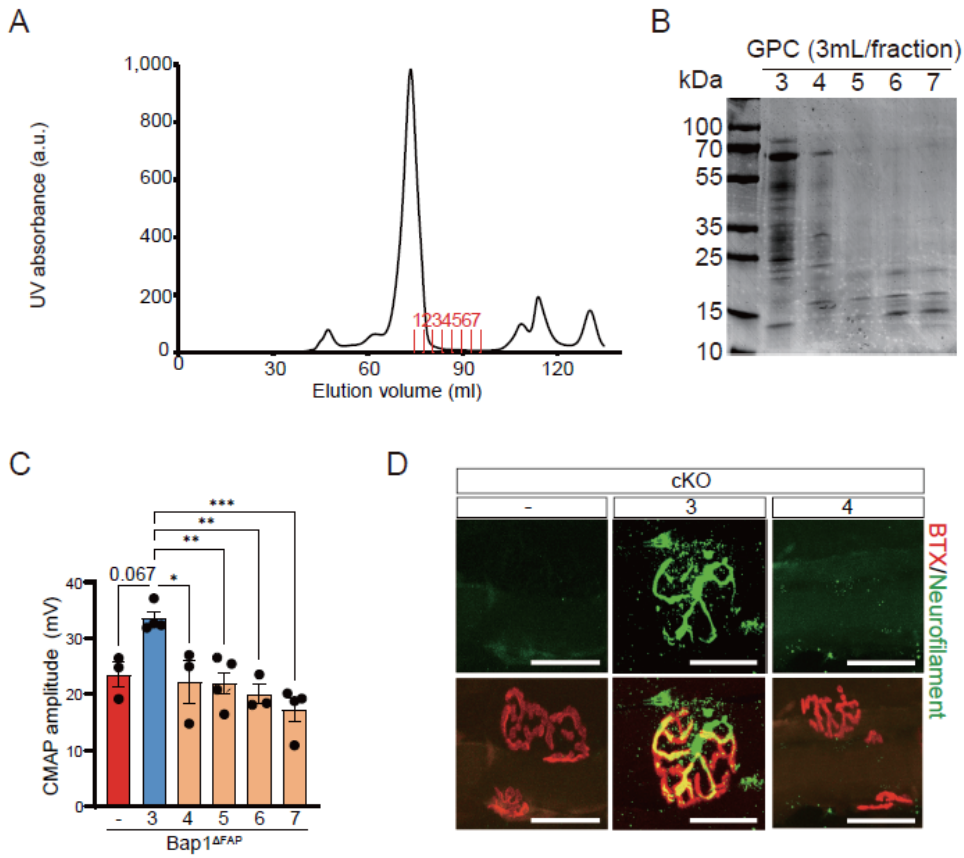
A
1,000
800
600
400
200
0
UV absorbance (a.u.)
1234567
0
30
60
90
120
Elution volume (ml)
B
GPC (3mL/fraction)
kDa
3 4 5 6 7
100
70
55
35
25
15
10
C
CMAP amplitude (mV)
0.067
*
**
**
***
40
30
20
10
0
- 3 4 5 6 7
Bap1ΔFAP
D
cKO
-
3
4
BTX/Neurofilament

Fig. 20. Venn diagram of genes satisfying the criteria of transcriptomic, and secretomic analyses, and size exclusion chromatography experiments. Only *granzyme E* satisfied all the criteria.

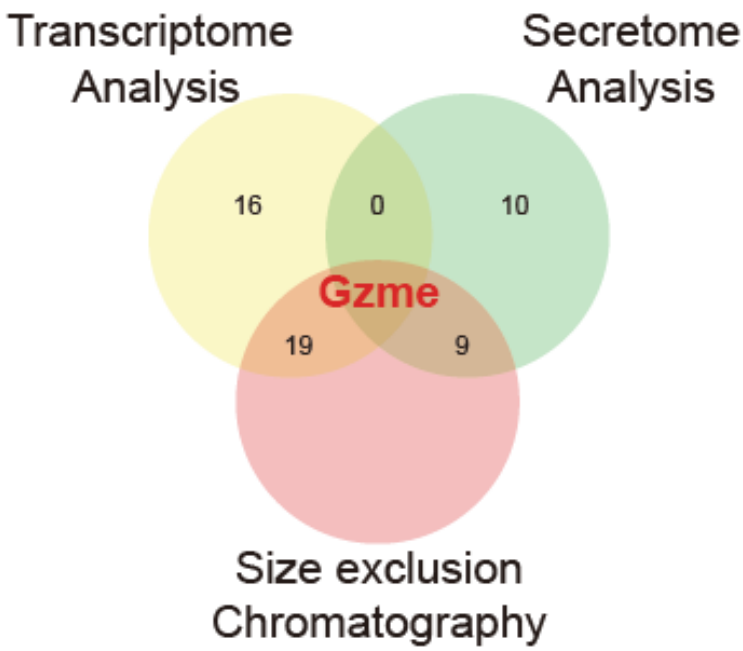
Transcriptome
Analysis
Secretome
Analysis
16
0
10
Gzme
19
9
Size exclusion
Chromatography

Fig. 21. Relative mRNA expression levels of *Bap1* and *granzyme E* (*Gzme*) in WT, ⊿Bap1, and SMN^{K186R}-overexpressing ⊿Bap1 FAPs. Expression of *granzyme E* is downregulated by Bap1 deletion and upregulated by SMN^{K186R} overexpression. n = 3 biological replicates per group.; One-way ANOVA followed by Tukey's pairwise comparison post hoc test.; Data are presented as mean ± s.e.m.; **p<0.01, ***p<0.001, ****<0.0001; ns, not significant.

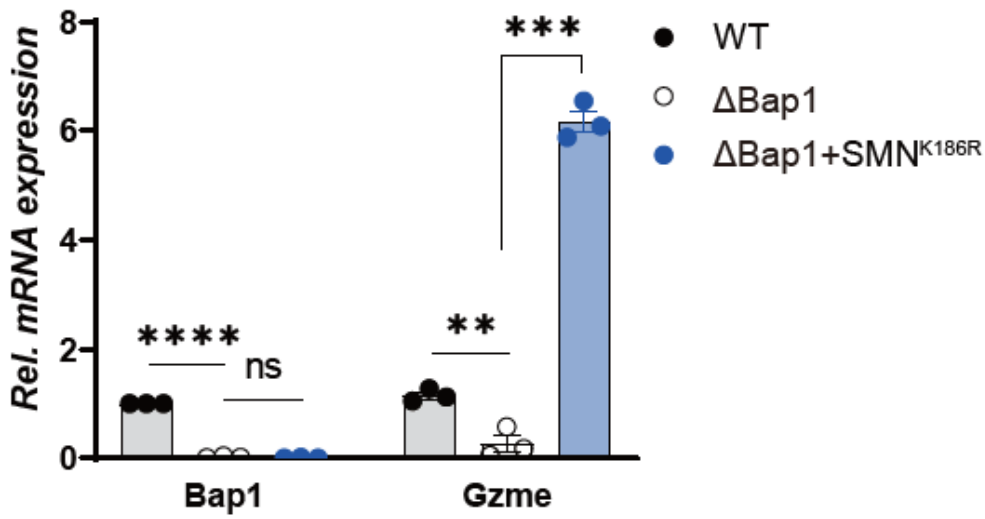
Rel. mRNA expression
8
6
4
2
0
****
ns
**
***
Bap1
Gzme
WT
ΔBap1
ΔBap1+SMN^K186R

Granzyme E rescues neuromuscular defects

To test whether granzyme E is indeed a secretory protein responsible for NMJ formation and function, causing neuromuscular abnormalities in cKO mice, the effect of granzyme E overexpression was analyzed in ⊿Bap1 FAPs (Fig. 22A). The transplantation of granzyme E-overexpressing ⊿Bap1 FAPs into cKO mice improved CMAP amplitude, whereas ⊿Bap1 FAP transplantation did not alleviate neuromuscular dysfunction (Fig. 22B).

To further confirm the direct effect of granzyme E on NMJ maturation, I produced granzyme E on a large scale using Chinese hamster ovarian (CHO) cells and treated cKO mice with granzyme E-CHO-CM (Fig. 23). Intriguingly, treatment with granzyme E-CHO-CM was sufficient to completely restore the decrease in CMAP in cKO mice (Fig. 24). Furthermore, the treatment of cKO mice with purified granzyme E was sufficient to rescue the neuromuscular phenotypes completely. Hindlimb posture and abnormal hindlimb clasping in cKO mice returned to normal after treatment with purified granzyme E (Fig. 25A, B). The NMJ structures, including the AChR endplate area and innervation status, were also rescued by granzyme E treatment (Fig. 26A-C). Accordingly, granzyme E treatment increased the CMAP amplitude in cKO mice (Fig. 26D). Granzyme E treatment also prevented the death of spinal motor neurons observed in cKO mice (Kim et al., 2022) (Fig. 27A, B). These data firmly support that lateral plate mesoderm-originated muscle FAPs secrete

granzyme E, affecting NMJ maturation and neuromuscular functions systemically.

Fig. 22. Rescue of neuromuscular defects in cKO mice by granzyme E-overexpressed ⊿Bap1 FAPs. (A) Transplantation schematics for granzyme E-overexpressing ⊿Bap1 FAPs in TA and GA muscles of cKO mice. FAPs were isolated from *Rosa*^{CreER};*Bap1*$^{f/f}$ mice and treated with lentivirus containing granzyme E_IRES_tdTomato transgene (Gzme_IRES_tdT) and 4-OHT to obtain granzyme E-overexpressing ⊿Bap1 (⊿Bap1+Gzme) FAPs. ⊿Bap1, and ⊿Bap1+Gzme FAPs were injected into the right TA and GA of the cKO mice. (B) Quantification of the CMAP amplitude in GA muscles from the indicated mice. Decrease of CMAP amplitude in cKO mice were rescued by granzyme E-overexpressed ⊿Bap1 FAPs.

A

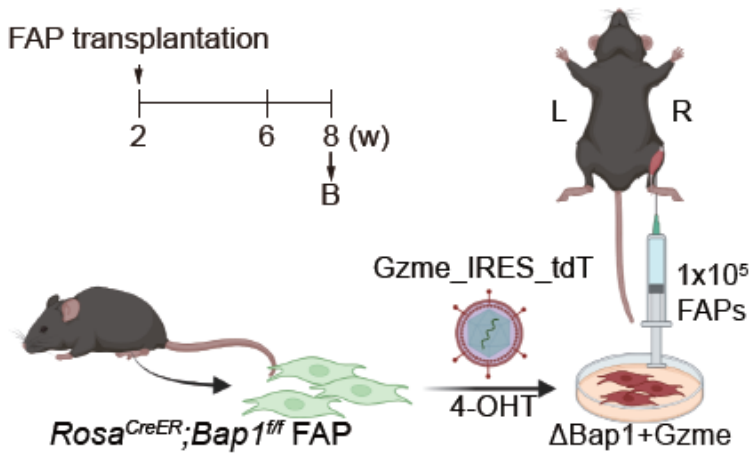
FAP transplantation
2
6
8 (w)
B
L
R
Gzme_IRES_tdT
1x10⁵
FAPs
4-OHT
RosaCreER;Bap1f/f FAP
ΔBap1+Gzme

B

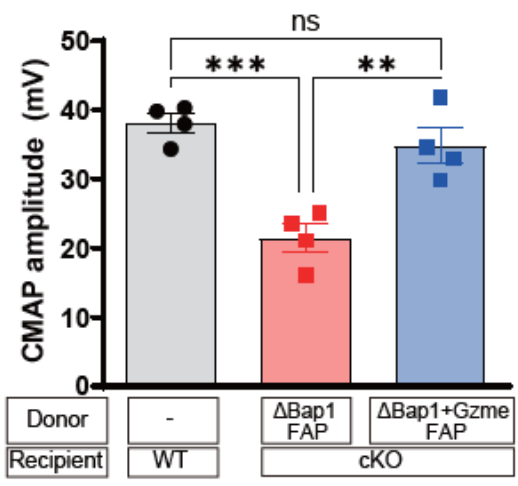
ns
***
**
CMAP amplitude (mV)
50
40
30
20
10
0
Donor
-
ΔBap1 FAP
ΔBap1+Gzme FAP
Recipient
WT
cKO

Fig. 23. Experimental scheme for granzyme E-overexpressing CHO-CM or purified granzyme E treatment in cKO mice. CHO cells were transduced with lentivirus containing 6xHis-Xpress tagged granzyme E transgene (Gzme-6xHis-Xpress), and CM was encapsulated in PLGA microparticles for the CHO-Gzme CM experiment (blue). Recombinant granzyme E was purified using Ni-NTA from CHO-Gzme CM and encapsulated into PLGA microparticles for purified granzyme E tests (green).

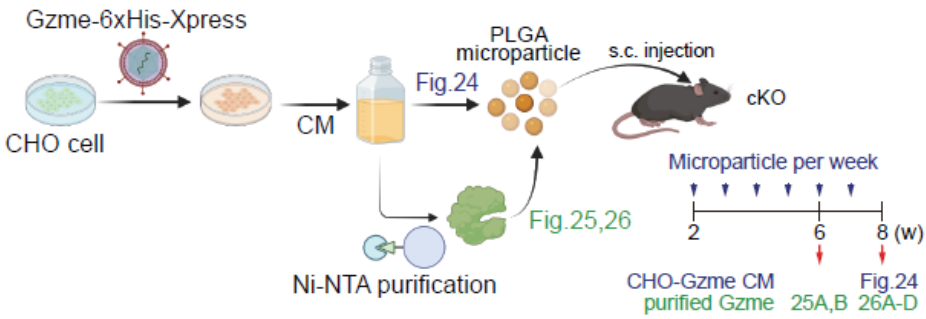
Gzme-6xHis-Xpress
CHO cell
CM
Fig.24
PLGA
microparticle
s.c. injection
cKO
Ni-NTA purification
Fig.25,26
Microparticle per week
2
6
8 (w)
CHO-Gzme CM
purified Gzme
25A,B
Fig.24
26A-D

Fig. 24. Quantification of CMAP amplitude in GA muscles from WT, CHO-WT, and CHO-Gzme CM-treated cKO mice. n = 4 animals per group. Each dot represents an individual mouse or a muscle; One-way ANOVA followed by Tukey's pairwise comparison post hoc test.; Data are presented as mean ± s.e.m.; *p<0.05, **p<0.01; ns, not significant.

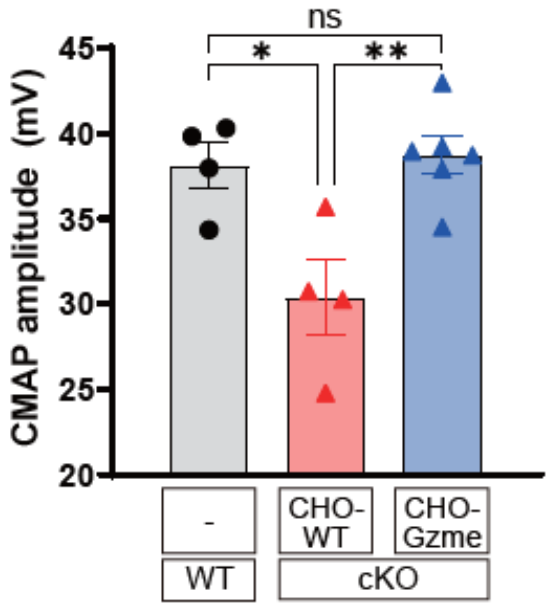
ns
*
**
45
40
35
30
25
20
CMAP amplitude (mV)
-
CHO-WT
CHO-Gzme
WT
cKO

Fig. 25. Recombinant granzyme E treatment ameliorated the dehavioral defects in cKO mice. (A) Representative images of the tail suspension test of cKO mice treated with or without purified granzyme E. (B) Quantification of abnormal hindlimb clasping time during 3 min of recording. Scales, 1 cm. n = 3 animals per group. Each dot represents an individual mouse or a muscle; One-way ANOVA followed by Tukey's pairwise comparison post hoc test.; Data are presented as mean ± s.e.m.; **p<0.01; ns, not significant.

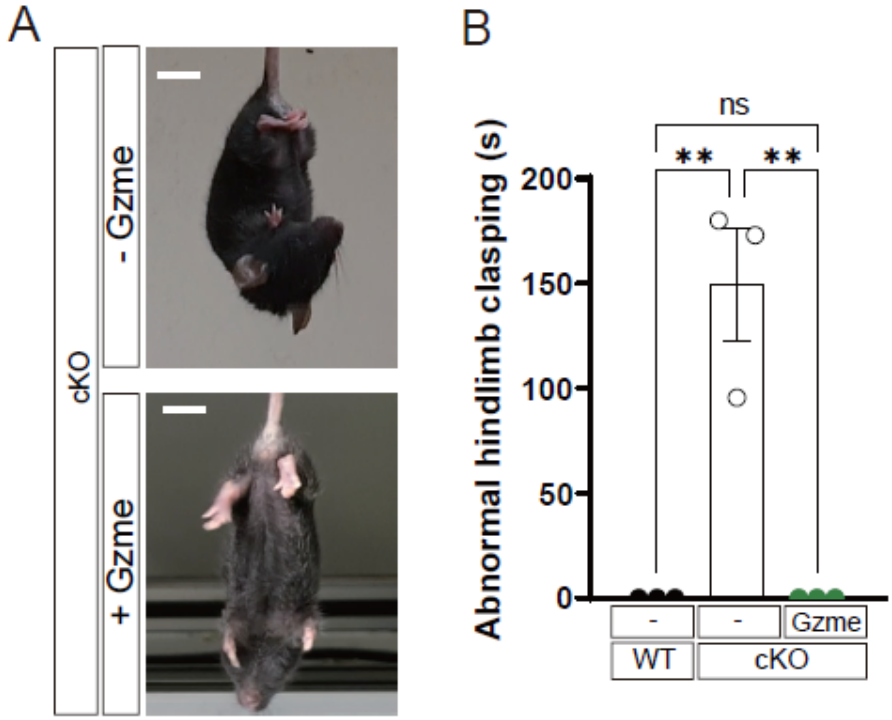
A
cKO
- Gzme
+ Gzme
B
Abnormal hindlimb clasping (s)
200
150
100
50
0
ns
**
**
-
-
Gzme
WT
cKO

Fig. 26. Recombinant granzyme E treatment restored neuronal defects in cKO mice. (A)Confocal images of bungarotoxin (BTX) and neurofilaments in the EDL muscles from WT, cKO, and cKO mice treated with granzyme E. (B) Quantification of the area occupied by acetylcholine receptor (AChR) staining and (C) degree of innervation of EDL muscles. (D) Quantification of CMAP amplitude of GA muscles from WT, cKO, and granzyme E-treated cKO mice. Scales, 50 μm (A). n = 3 (B-D) animals per group. Each dot represents an individual mouse or a muscle; One-way ANOVA followed by Tukey's pairwise comparison post hoc test (B-D). Two-way ANOVA followed by Tukey's pairwise comparison post hoc test; Data are presented as mean ± s.e.m.; *p<0.05, **p<0.01, ***p<0.001, ****p<0.0001; ns, not significant.

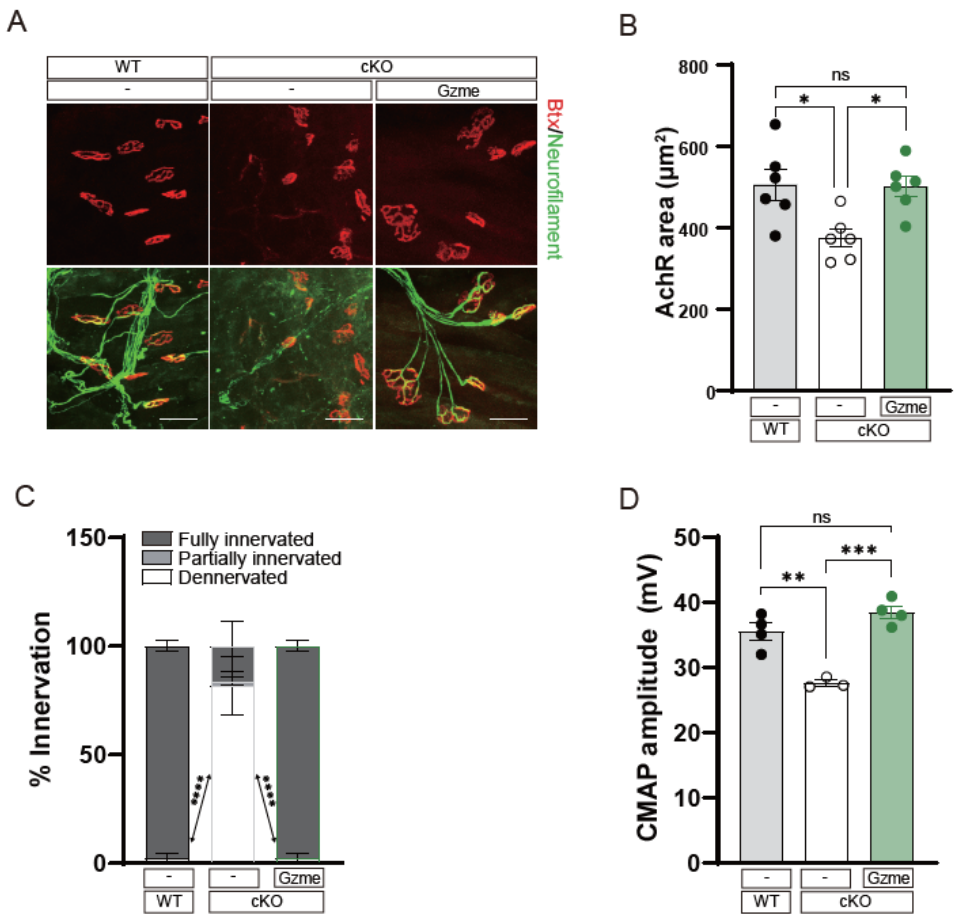
A
WT
cKO
-
-
Gzme
Btx/Neurofilament
B
AchR area (μm²)
800
600
400
200
0
ns
*
*
-
-
Gzme
WT
cKO
C
% Innervation
150
100
50
0
Fully innervated
Partially innervated
Dennervated
****
****
-
-
Gzme
WT
cKO
D
CMAP amplitude (mV)
50
40
30
20
10
0
ns
**
***
-
-
Gzme
WT
cKO

Fig. 27. Prevention of motor neuron death by granzyme E treatment.

(A, B) Immunohistochemical images (A) and quantification of choline acetyltransferase (ChAT) and neuronal nuclei (NeuN) staining in the ventral horn region of the L5 spine in WT, cKO, and granzyme E-treated cKO mice (B). Cells co-stained with ChAT and NeuN were quantified as motor neurons (MNs). n = 3 (B) animals per group. mean ± s.e.m.; one-way ANOVA followed by Tukey's pairwise comparison post hoc test (B); **<0.01.

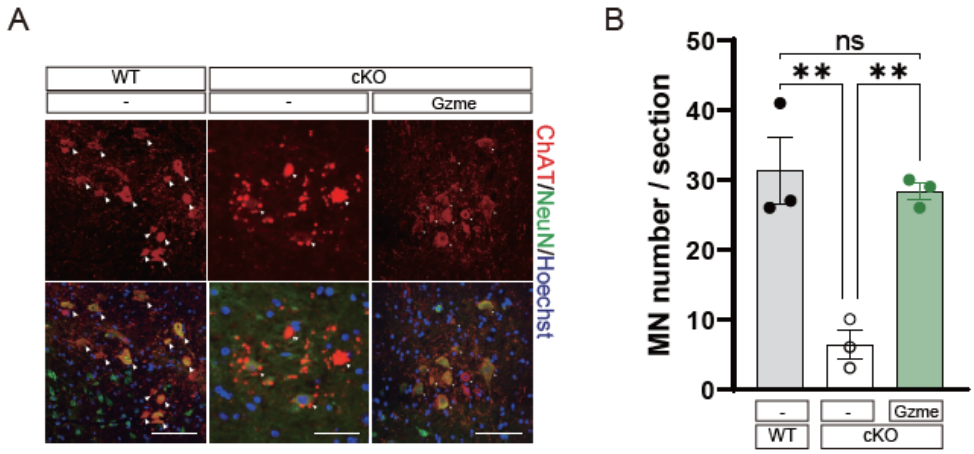
A
WT
cKO
-
-
Gzme
ChAT/NeuN/Hoechst
B
MN number / section
50
40
30
20
10
0
ns
**
**
-
-
Gzme
WT
cKO

Discussion

The relevance of NMJ defects in neuromuscular diseases, including spinal muscular atrophy (SMA) and ALS, have been suggested previously (Boido and Vercelli, 2016; Campanari et al., 2016; Moloney et al., 2014). In SMA model mice, synaptic defects such as the impaired plaque-to-pretzel transition of AChR clusters, neurofilament accumulation, poor terminal arborization, and immature endplates have been observed (Boido and Vercelli, 2016). These defects precede denervation and death of motor neurons, resulting in muscle weakness and atrophy (Boido and Vercelli, 2016). NMJ defects in ALS are identified at a very early stage prior to symptom onset, implicating the role of dysfunctional NMJ in the onset and progression of muscular disease (Moloney et al., 2014). Here, I suggest that the systemic factor granzyme E mediated the regulation and maturation of NMJ, a novel concept that can be further explored as a therapeutic approach to muscular diseases. Mesenchymal cells have been known to avoid allogeneic immune rejection (Ryan et al., 2005), which makes human FAPs (hFAPs) a good therapeutic candidate for muscular disorders caused by defects in NMJs. To extend this study over to human therapies, the function of hFAPs and their secretory factors in the neuromuscular systems need to be further analyzed.

During skeletal muscle development, T-cell factor 4 $(Tcf-4)^+$ mesenchymal cells originate from the somatic lateral plate mesoderm, migrate into the limb field, intermingle with muscle progenitors

derived from dermomyotome, and support muscle patterning and myogenic differentiation by providing pro-myogenic niches (Kardon et al., 2003; Mathew et al., 2011), and eventually develop into FAPs. It has been suggested that the mesenchymal cells can support neural functions such as neural cell growth, regeneration, migration, and axonal guidance to target sites (Mukhamedshina et al., 2019). However, the role of FAPs in motor neuron function remains unidentified. Here, I showed that FAPs play a pivotal role in skeletal muscle innervation by motor neurons through the secretion of granzyme E in a systemic manner. Although previous studies have demonstrated the cytotoxic functions of granzyme family endopeptidase (Bots and Medema, 2006; Granville, 2010; Hiroyasu et al., 2021; Mark S. Pasternack and Herman N. Eisen, 1985; Voskoboinik et al., 2015), the detailed mechanism by which granzyme E affects the neuromuscular systems remains elusive. Further investigations on the molecular mechanisms underlying the granzyme E-mediated regulation of NMJ would help better understand the neuromuscular systems and its therapeutic application for NMJ-related muscle weakness.

Granzymes are chymotrypsin-like serine proteases consisting of 2 subfamilies of 11 proteins: granzyme A, B, C, D, E, F, G, H, K, M, and N. Many studies have reported the cytotoxic functions of granzymes including granzyme A, B, C, F and M (Bots and Medema, 2006; Chowdhury et al., 2006; Johnson et al., 2003; Kelly et al., 2004; Martinvalet et al., 2005; Shi et al., 2009; Trapani and Sutton, 2003). Meanwhile, recent studies have demonstrated the non-cytotoxic

function of granzyme proteins (Rönnberg et al., 2013; Tsai et al., 2010), suggesting that further studies on the non-cytotoxic functions of individual granzymes are required for an in-depth understanding of how granzyme proteases regulate cellular processes. However, the low and restricted expression of granzyme E in FAPs (data not shown) and its sequence similarity with granzyme D posed a great challenge in the study of the function of granzyme E. I report the unique expression of granzyme E in FAPs and its functional relevance in NMJ maturation and the neuromuscular system.

In summary, muscle FAPs derived from the lateral plate mesoderm secrete granzyme E, a novel protein required for the proper maturation and function of NMJ. The NMJ is a specialized synapse composed of nerve terminals, muscle fibers endplates, and surrounding terminal Schwann cells (Joshua R. Sanes and Jeff W. Lichtman, 2001; Wu et al., 2010). I suggest that mesenchymal FAPs are indispensable components in the maturation, maintenance, and function of NMJs. By establishing a functional link between neuromuscular systems and muscle mesenchymal FAPs, this study provides an understanding of neuromuscular system regulation.

Perspectives

In mammals, skeletal muscle consists up to ~50% of total body mass, and its motor activity, regulation of body temperature, and metabolism are critical for the survival of the organism. Skeletal muscles are controlled by neurotransmitters released from the motor neurons and their recognition by acetylcholine receptors on muscle fibers. Abnormalities of NMJs are common pathological causes of muscle diseases including SMA, ALS, and congenital myasthenic syndromes (Harding et al., 2015; Kariya et al., 2008; Moloney et al., 2014; Pollari et al., 2014; Valsecchi et al., 2015). Many researchers have investigated the cellular components and molecular mechanisms of NMJ regulation such as formation, maturation, maintenance, and re-establishment (Rodríguez Cruz et al., 2020). However, interactions between NMJ and FAPs have not been thoroughly studied. Kim et al. previously suggested FAPs as a novel and critical regulator of NMJ maturation on distal muscles (Kim et al., 2022). In this study, I addressed a key question of how FAPs control NMJ maturation in whole body scale. By analyzing the transcriptome and secretome of Bap1-null and Smn-overexpressed FAPs, I revealed the novel function of granzyme E as a systemic regulator of NMJ maturation and maintenance. Since most studies on NMJ regulations focus on autocrine or paracrine factors regulating local NMJs (Baudet et al., 2008; Fox et al., 2007; Gesemann et al., 1995; Hayworth et al., 2006; Henriquez et al., 2008; Jing et al., 2009; McCabe et al., 2004;

Nishimune et al., 2008), this study will open a new research field on systemic regulation of NMJ. Further investigations on the molecular mechanisms of global control of NMJ can show important insights on the development of therapies for NMJ-related muscle diseases.

Acknowledgement

I specially appreciate
Ji-Hwan Park and Daehee Hwang for the analysis of RNA sequencing data,
Sanghee Shin and Jong-Seo Kim for analyses of secretome and mass spectrometric data,
Kyoo Heo and Yeong-Jae Seok for chromatography and protein fractionation.

Material & Methods

Animals

Prrx1-Cre (005584) and *Rosa-CreER* (008463) mice were obtained from The Jackson Laboratory (Bar Harbor, ME, USA). *Bap1*$^{f/f}$ mice were generated using the gene-trap ES cell line (HEPD0526_2_G01) made by EUCCOM (the Gene-trap consortium). Gene trap cassette was integrated within the fifth intron of murine Bap1 locus and LoxP site was inserted within the twelfth intron of murine Bap1 locus (previously described by Kim et al., 2022). The resulting Bap1 floxed mice were crossed with *Prrx1-Cre* mice to generate *Prrx1-Cre;Bap1*$^{f/f}$ mice. Cre-mediated deletion of these exons resulted in a frameshift mutation, leading to premature termination of the mouse Bap1 open reading frame. Bap1 floxed mice were crossed with *Rosa-CreER* mice to generate *Rosa-CreER;Bap1*$^{f/f}$ mice. All mouse lines were backcrossed into a C57BL/6J background and were housed under specific pathogen-free conditions and handled according to the guidelines of the Institutional Animal Care and Use Committee (IACUC) at Seoul National University. Experiments were carried out with male and female mice, except for whole transcriptomic analysis, where only male mice were used. No sex-specific differences were observed.

Histochemistry and immunohistochemistry

Tibialis anterior (TA) and *triceps brachii* (Triceps) muscles were

embedded in the OCT compound (Sakura Fineteck, Torrance, CA, USA), snap-frozen in liquid nitrogen, and stored at -80° C prior to sectioning. Embedded muscles were sliced into 7 mm-thick sections using a cryostat (Leica, Wetzlar, Germany). For the staining of muscle sections, randomly selected slides at the same sectional position between groups were fixed in 4% PFA. Fixed slides were blocked for 1 hour at room temperature with blocking buffer (5% bovine serum albumin in PBS) and incubated for 2 hours with rat anti-laminin (abcam, ab11576, 1:1000 dilution) and rabbit anto-TurboGFP (ThermoFisher, PA5-22688, 1:1000 dilution) in blocking buffer at room temperature. After incubation, slides were washed with PBS-T (0.1% Triton X-100 in PBS) 3 times and were incubated for 1 h with 1:1000 dilution of Alexa Fluor 594-conjugated anti-rat IgG, Alexa Fluor 488-conjugated anti-rabbit IgG and 1:4000 dilution of Hoechst 33342 (Thermo Fisher Scientific).

For spinal cords, L5 spinal cords were isolated and fixed in 4% PFA overnight at 4° C and were incubated in 15% sucrose solution following 30% sucrose solution until the spinal cords sank. Cryoprotected spinal cords were embedded in the OCT compound, snap-frozen in liquid nitrogen, and stored at -80° C until sectioning. Embedded spinal cords were sectioned into 7 mm-thick using cryostat. For staining of spinal cords, slides of spinal cords were washed with PBS and permeabilized with cold methanol for 30 minutes at 4° C. Samples were washed 2 times with PBS-T and 1 time with PBS for 7 minutes each. Afterward, slides were incubated in mouse IgG blocking reagent (Vector laboratories, Burlingame, CA,

USA) for 1 hour at room temperature to block endogenous mouse immunoglobulin, and washed 3 times with PBS for 7 minutes each. Sections were then blocked with protein concentrate solution (Vector laboratories, Burlingame, CA, USA) for 1 hour at room temperature. Slides were incubated overnight at 4° C with the primary antibody for NeuN (Chemicon, MAB377, 1:1000 dilution) and ChAT (Sigma-Aldrich, AB144P, 1:100 dilution). The next day, Slides were washed and incubated with secondary antibody (Alexa Fluor 594-conjugated anti-goat IgG, 1:1000) at room temperature for 1 hour. Sections were washed 3 times with PBS-T for 5 minutes each and blocked with blocking solution (5% goat serum in PBS) for more than 1 hour at room temperature to block remaining anti-goat binding sites. Sections were washed 3 times with PBS for 5 minutes each and incubated with secondary antibody (Alexa Fluor 488-conjugated anti-mouse IgG, 1:1000) and Hoeschst 33342 at room temperature for 1 hour. Slides were washed 3 times with PBS-T for 5 minutes and mounted with VECTASHIELD mounting medium (Vector laboratories, Burlingame, CA, USA) and covered by the coverslip.

For staining of the innervated neuromuscular junction (NMJ), TA, triceps, *extensor carpi radialis*, *flexor carpi radialis* muscles were dissected, fixed overnight in 4% PFA at 4 ° C and quenched with 0.1M glycine in PBS for 1 hour at room temperature. Samples were washed three times with PBS and blocked with blocking buffer (5% BSA, 2% Triton X-100 in PBS) overnight at 4 ° C. Muscle bundles were incubated with rabbit anti- neurofilament M antibodies (Merck, AB1987, 1:1000 dilution) in 2% Triton X-100 in PBS for overnight

at 4 ° C. After three washes with 2% Triton X-100 in PBS, muscles were stained with Alexa Fluor 488-conjugated anti-rabbit IgG (1:1000), Alexa Fluor 555-conjugated bungarotoxin (1:1000) and Hoechst 33342 (1:4000) overnight at 4 ° C. Finally, muscle fiber bundles were washed three times with 2% Triton X-100 in PBS and mounted in VECTASHIELD mounting medium.

Limb muscle fibroadipogenic progenitor cell isolation

Isolation of limb muscle mesenchymal fibroadipogenic progenitor cells (FAPs) was performed according to a previously reported protocol (Gromova et al.) with minor modifications. Hindlimb and forelimb muscles were dissected and mechanically dissociated in Dulbecco' s modified Eagle' s medium (DMEM) containing 10% horse serum (Hyclone, Logan, UT, USA), collagenase II (800 units/mL; Worthington, Lakewood, NJ, USA), and dispase (1.1 units/mL; ThermoFisher Scientific, Waltham, MA, USA) at 37° C for 40 min. Digested suspensions were subsequently triturated by sterilized syringe with 20G1/2 needle (BD Biosciences, Franklin Lakes, NJ, USA), strained with 40㎛ cell strainer (SPL Lif eSciences, Pocheon, Korea) and washed with DMEM to harvest mononuclear cells. Mononuclear cells were stained with corresponding antibodies. All antibodies used in FACS analysis were listed in Table 1. To exclude dead cells, 7-Aminoactinomycin D (Sigma-Aldrich; St. Louis, MO, USA) was used prior to FACS analysis. Stained cells were analyzed and $7AAD^{-}Lin^{-}Vcam^{-}Sca1^{+}$

cells were isolated using a FACS Aria III cell sorter (BD Biosciences) with 4-way-purity precision. Isotype control density plots were used as a reference for positive gating.

FAP transplantation

$1*10^5$ FAPs were resuspended in PBS and immediately transplanted into TA and GA muscles of cKO mice that were littermates of donor mice. Control mice (wild-type and cKO mice) received the same volume of PBS.

Electromyography

Compound muscle action potentials (CMAP) were measured as previously described (Pollari et al., 2018). Briefly, mice were anesthesized using tribromoethanol (avertin; Sigma Aldrich; St. Louis, MO, USA) and placed on the insulation plate. Stimulating electrodes were subcutaneouly placed on both sides of sciatic notch and the ground electrode was placed under the skin of tail. Reference and recording electrodes were inserted subcutaneously next to Achilles tendon and GA muscle, respectively. CMAP was recorded under the recurrent stimuli (1 pulse/s) until reach the supramaximal CMAP amplitude (2-30 mA stimulus). The amplitude of 10 consecutive CMAP peaks were analyzed and averaged. CMAP amplitudes were measured in triplicate per muscle to obtain CMAP amplitude of specific muscle.

Tail suspension test

All behavior tests were performed by the observer blinded to the mouse genotypes and descriptions. To evaluate motor functions, previous methods were modified and applied (Pollari et al., 2018). For the tail suspension test, mice were suspended by their tail for 4 min. Each mouse was adapted to inverted position for 1 min. The time that individual mouse showed abnormal hind-limb clasping during 3 min of tail suspension was measured. Abnormal hind-limb clasping was determined by the proximity of hindlimbs with postural abnormalities. All behavior tests were conducted between 19:00 and 21:00 to exclude any unwanted circadian effects.

Cell culture, transfection and plasmids

Freshly isolated FAPs of indicated genotypes were cultured at 37 ° C in alpha-MEM (Hyclone) supplemented with ZellShield (Minerva Biolabs; Skillman, NJ, USA) and 20% FBS (Hyclone). HEK293T cell line (ATCC, Manassas, VA) was grown at 37 ° C in DMEM (Hyclone) supplemented with ZellShield and 10% FBS. The cell line was regularly tested for mycoplasma contamination. All transfections were performed using polyethyleneimine (PEI; Polysciences, Warrington, PA, USA). Full length and point-mutated constructs of human SMN were subcloned into the pcDNA4-HisMAX vector and pLVX vector. SEC61B-TurboID construct was kindly provided by Dr. Hyun-Woo Rhee (Kim et al., 2021). SEC61B-TurboID was cloned into pLVX vector to produce lentivirus required

for FAP transduction. Granzyme E coding sequence was amplified from freshly isolated FAP cDNA and cloned into pLVX vector. Six tandem histidine tag (6xHis) and Xpress tag coding sequence or IRES-tdTomato sequence was inserted on the C-terminus of Granzyme E protein coding sequence.

For Bap1 deletion under Rosa-CreER, FAPs were cultured with 1 μM 4-Hydroxytamoxifen (4-OHT). Equal concentration of ethanol was used as a control. Culture media was replaced by alpha-MEM supplemented with ZellShield and 20% FBS 24 hours after exposure to 4-OHT. Subsequent deletion of Bap1 gene was confirmed by qRT-PCR.

Lentivirus packaging and transduction TurboGFP labelling

With psPAX2 (4.5mg) and pMD2.G (1.5mg), lentiviral pLVX-Smn^{WT}-IRES-tdTomato, pLVX-Smn^{K186R}-IRES-tdTomato or pGIPZ_TurboGFP (6mg) vectors were co-transfected into HEK293T cells using PEI. The cultured supernatants containing virus particles were harvested 48 hours post-transfection, filtered through 0.45mm filters and concentrated using a Lenti-X concentrator (Takara, Kyoto, Japan). For virus titration, quantitative PCR (qPCR) analysis was performed. For the standard curve, transgene expressing plasmid was digested with restriction enzymes and run on a 2% agarose gel at 200 volts for 20min. A single fragment of defined size was purified using a PCR purification kit, and

measured for the DNA concentration. DNA was finally diluted to a concentration of $1*10^9$ vg (vector genome)/mL. Standard plasmid was 10-fold serially diluted from $1*10^7$ vg/mL to $1*10^1$ vg/mL in triplicates. For serially diluted template DNA, 2mL of the concentrated lentiviral stock was mixed with 198mL of DNaseI buffer containing 2mL of DNaseI in a PCR tube and incubated for 30min at 37° C. After inactivation of DNaseI, the solution was 10-fold serially diluted from $1*10^{-3}$ vg/mL to $1*10^{-5}$vg/mL in triplicates. qPCR analysis of diluted DNA was conducted to calculate the concentration of lentivirus. For virus transduction, freshly isolated or cultured FAPs were suspended centrifuged at 500g for 5 min and the supernatant was aspirated. The cell pellet was resuspended with fresh media containing lentiviral stock with 4mg/mL polybrene (Santa Cruz Biotechnology, Dallas, TX, USA) and then incubated in an appropriate culture dish for 16 hours at 37° C. After incubation, viral media were replaced by alpha-MEM (Hyclone) supplemented with ZellShield (Minerva Biolabs; Skillman, NJ, USA) and 20% FBS (Hyclone). The final $5.0*10^8$ vg/mL titer lentiviral particles were used.

Conditioned media collection

Indicated FAPs were cultured until passage 4. When they reach 100% confluency, culture media was aspirated and washed twice with PBS. Fresh alpha-MEM was added 20mL per 150ϕ culture plate. After 24 hours, conditioned media was collected and filtered using 0.45㎛

bottle top vacuum filter (Corning; NY, USA) and dialyzed using 3 kDa MWCO SpectraPor Regenerated Cellulose membrane (Repligen; MA, USA) with triple distilled water at 4° C for 3 days. Protein concentration of dialyzed CM was measured using Pierce BCA assay (Thermo Fisher; MA USA), aliquoted, lyophilized and stored at −80° C.

Preparation of PLGA microparticle

PLGA (Poly(D,L−lactide−co−glycolide)) microparticles were encapsulated as previously described (Kang et al., 2019) with some modifications. Briefly, 25 mL dose of CM, BSA and triple distilled water were mixed to form 2mg protein in 2mL aqueous solution. One−mL of 2.5% (w/v) PLGA, 50:50, Polysciences Cat.26269; Warrington, PA, USA) solution dissolved in dichloromethane (Sigma−Aldrich) was added on the top of protein−containing aqueous solution. Aqueous and organic phases were vigorously emulsified under 60% amplitude sonicator (Sonics VCX 130; Newtown, CT, USA) for 100 seconds. The emulsion solution was dropped into 20mL of 0.5% (w/v) PVA (Sigma−Aldrich) solution under 60% amplitude sonicator on ice. After 45 seconds, the double emulsion solution was incubated for 1 hour with continuous stirring at 700rpm at 25° C. The hardened microparticles were flowed through 40㎛ strainer and centrifuged at 13000g for 10 minutes. Microparticles were resuspended in triple distilled water under bath sonicator (Branson Ultrasonics; CT, USA), washed 3 times,

lyophilized and stored at −80° C until use. Lyophilized microparticles were resuspended in 50 or 100 μL of PBS and subcutaneously injected under the neck skin.

RNA extraction and measurement of mRNA expression

Total RNA was extracted from cultured FAPs with TRIzol Reagent (Life Technologies, Carlsbad, CA, USA) and analyzed by qRT−PCR. First−strand complementary DNA was synthesized from 0.1−1 μg of RNA using ReverTra Ace (Toyobo, Osaka, Japan) containing random oligomer according to the manufacturer's instructions. qRT−PCR was performed with ORA SEE qPCR mix (HighQu Gmbh; Germany) using specific primers against indicated genes. Relative mRNA levels were determined using the $2^{-\Delta\Delta Ct}$ method and normalized to β−actin. Primers are listed in Supplementary Table 1.

Transcriptomic analysis

RNA sequencing analysis of WT, ⊿Bap1, SMN^{WT}−overexpressed ⊿Bap1, and SMN^{K186R}−overexpressed ⊿Bap1 FAPs was conducted. Total RNA was extracted from FAPs using TRIzol Reagent (Life Technologies, Carlsbad, CA, USA) and the TruSeq Stranded mRNA LT Sample Prep Kit was used to generate Illumina RNA−seq libraries, according to the manufacturer's instructions. RNA−seq libraries were sequenced as paired−ends on an Illumina platform. The adaptors were removed from the raw reads using cutadpt (ver 3.4), and the resulting reads were then aligned to the mouse reference

genome (GRCm39) using the STAR aligner (ver 2.7.9a) (Dobin et al., 2013). Transcripts were quantified based on gene count feature (GRm39.105.gtf) using htseq-count, and transcript levels were finally normalized with the variance stabilizing transformation method (Anders and Huber, 2010) in DESeq2 (ver 3.12).

Using the normalized transcript levels, differentially expressed genes (DEGs) were identified using a previously reported integrative statistical testing method (Chae et al., 2013) for the following comparisons: 1) ⊿Bap1 versus WT and 2) SMN^{K186R}-overexpressed ⊿Bap1 versus SMN^{WT}-overexpressed ⊿Bap1. In brief, I first computed $\log_2$-ratios for three pairs of samples between two conditions in each comparison and then calculated T-statistic values of individual genes using one-sample Student's t-test and also the median $\log_2$-ratios. I generated empirical null distributions of T-statistic value and $\log_2$-median-ratios ($\log_2$-fold-changes) by randomly permuting all samples and computing T-statistic values and $\log_2$-fold-changes for the permuted samples (1000 times). Based on two null distributions, for each gene, adjusted p values for the observed T-statistic value (P_t) and $\log_2$-fold-change (P_f) were computed, and then merged into a combined adjusted p values (P_{com}) using Stouffer's method (Hwang et al., 2005). Finally, the genes with $P_{com} < 0.05$ and absolute $\log_2$-fold-changes larger than a 95th percentile value from the above fold-change null distribution (⊿Bap1 versus WT: 1.42-fold and SMN^{K186R}-overexpressed ⊿Bap1 versus SMN^{WT}-overexpressed ⊿Bap1: 1.32-fold) were selected as DEGs.

Proteome digestion and enrichment of biotinylated peptides

Lyophilized CM was resolubilized with 1 mL of 8 M urea (Sigma-Aldrich, U5378) in 50 mM ammonium bicarbonate (ABC, Sigma-Aldrich, A6141). Concentration of protein was measured by BCA assay. Samples were denatured at 650 rpm for 1 h at 37° C using Thermomixer (Eppendorf). The samples were reduced by adding dithiothreitol (Sigma-Aldrich, 43816) to 10 mM final concentration and incubated at 650 rpm for 1 h at 37° C using Thermomixer. The samples were alkylated by adding iodoacetamide (Sigma-Aldrich, I1149) of 40 mM to final concentration and mixed at 650 rpm for 1 h at 37° C using Thermomixer. The samples were diluted eight times using 50 mM ABC. CaCl2 (Alfa aesar, 12312) was added to 1 mM final concentration. Trypsin (Thermoscientific, 20233) was added to each sample (50:1 w/w). Samples were incubated for digestion at 650 rpm for 6-18 h at 37° C using Thermomixer.

Digested peptide samples were centrifuged at 15,000 × g for 15 min to remove insoluble material. Then, biotinylated peptides were enriched by adding 150 μL of streptavidin beads (Pierce, 88817) to the sample. The samples were rotated for 1 h at room temperature. The flow-through fraction was kept, and the beads were washed twice with 2 M urea in 50 mM ABC followed by washing with pure water. Enriched biotinylated peptides were treated with PNGase F (NEB, P0704) on-bead by following manufacture' s non-denaturing protocol. Then the beads were washed twice with 2M urea in 50mM

ABC followed by the washing with pure water. Finally, biotinylated peptides were eluted by adding 200 μL of elution buffer (80% acetonitrile (Sigma-Aldrich, 900667), 0.2% TFA (Sigma-Aldrich, T6508), and 0.1% formic acid (Thermoscientific, 28905)) to the sample and incubated at 60° C for 5 min. Each supernatant was transferred to new tubes. Elution step was repeated four times. Speed Vac (Eppendorf) was used to dry the combined eluted fractions. Samples can be stored ate −20° C or injected to mass spectrometry directly.

LC-MS/MS analysis of enriched peptide samples

Analytical capillary columns (100 cm x 75 μm i.d.) and trap columns (2 cm x 150 μm i.d) were packed in-house with 3 μm Jupiter C18 particles (Phenomenex, Torrance). The long analytical column was placed in a column heater (Analytical Sales and Services) regulated to a temperature of 45° C. NanoAcquity UPLC system (Waters, Milford) was operated at a flow rate of 300 nL/min over 2 h with linear gradient ranging from 95% solvent A (H2O with 0.1% formic acid) to 40% of solvent B (acetonitrile with 0.1% formic acid). The enriched samples were analyzed on an Orbitrap Fusion Lumos mass spectrometer (Thermo Scientific) equipped with an in-house customized nanoelectrospray ion source. Precursor ions were acquired (m/z 300-1500) at 120 K resolving power and the isolation of precursor for MS/MS analysis was performed with a 1.4 Th. Higher-energy collisional dissociation (HCD) with 30% collision

energy was used for sequencing with auto gain control (AGC) target of 1e5. Resolving power for acquired MS2 spectra was set to 30 k at with 200 ms maximum injection time.

MS data processing and protein identification

All MS/MS data were searched by MaxQuant (version 1.6.5.0) with Andromeda search engine at 10 ppm precursor ion mass tolerance against the mouse (mus musculus) proteome database (55,413 entries, UniProt (http://www.uniprot.org/), retrieved;2020-04-14). The label free quantification (LFQ) and Match Between Runs were used with the following search parameters: semi-trypic digestion, fixed carbaminomethylation on cysteine, dynamic oxidation of methionine, protein N-terminal acetylation with biotin labels of lysine residue. Less than 1% of false discovery rate (FDR) was obtained for unique labeled peptide and as well as unique labeled protein. LFQ intensity values were log-transformed for further analysis and missing values were filled by imputed values representing a normal distribution around the detection limit. To impute the missing value, first, the intensity distribution of mean and standard deviation was determined, then for imputation values, new distribution based on Gaussian distribution with a downshift of 1.8 and width of 0.3 standard deviations was created for total matrix.

Size exclusion chromatography

Eighty-milliliter lyophilized CM was resuspended with 1 ml distilled

water. Samples were centrifuged at 10,000 rpm for 10 min and supernatants were loaded onto a Hiload 16/60 Superdex 200 pg gel-filtration column (GE Healthcare; Il, USA) equilibrated with 20 mM Tris-HCl (pH 8.0), 50 mM NaCl, 5 mM b-mercaptoethanol. Three-milliliter fractions were collected every 3 min from 75 min to 147 min. Protein-containing fractions were loaded on SDS-PAGE gel and Coomassie stained to determine the size of protein contents.

Ni-NTA purification

6xHis-tagged Granzyme E was purified using Ni-NTA agarose resin (Qiagen; MD, USA) according to the manufacturer' s instruction. Briefly, CM of 6xHis-Granzyme E expressed CHO was diafiltrated and concentrated into 1/10 volume using 5kDa MWCO Labscale TFF system (Merck). Prior to the binding of Ni-NTA, buffer was changed to 20 mM Tris pH 8.0, 150 mM NaCl dialysis buffer, subsequently bound to Ni-NTA for 40 minutes at 4° C. Unbound proteins were washed 3 times with dialysis buffer with 20mM imidazole. 6xHis-tagged proteins were eluted under dialysis buffer with 250 mM imidazole. Elution of tagged protein was confirmed by SDS-PAGE and Coomassie staining.

Optical systems

Immunofluorescence images were acquired using a EVOS FL Auto 2 (Thermo Fisher, Waltham, MA, USA) or a Zeiss confocal system Leica SP8. Images were acquired thirty distinct cross-sectional

fields of each L5 spinal cord sections and the section containing the highest number of $ChAT^+$ motor neurons in groups were quantified and statistically analyzed. To quantify endplate area, acetylcholine receptor cluster size and innervated NMJ, a minimum of 30 NMJs from each muscle were captured by Leica SP8 confocal laser scanning microscopy. LasX software was used to obtain maximal projections and merged images of the red and green channels. Endplate area was quantified by the surface area measurement of polygon circumscribing the bungarotoxin stained area using LasX software. Acetylcholine receptor cluster size measurement and innervation status was performed as previously described (ref). In brief, area of bungarotoxin (red channel), neurofilament (green channel) and colocalization of two channels were measured using Image J software. NMJs with 0%, 0~20%, and >20% overlapping area of bungarotoxin and neurofilament signals were classified as denervated, partially innervated, and fully innervated NMJs (20% was set as a criterium for full innervation since neurofilament is typically stained much thinner than bungarotoxin).

Statistical analysis

All statistical analyses were performed using R software (R-4.1.2) and GraphPad Prism 9 (GraphPad Software). Continuous variables were tested for normal distribution by using the Shapiro-Wilk test for $n<5$ datasets and Kolmogorov-Smirnov test for $n\geq5$ datasets. For comparison of significant differences in multiple groups,

statistical analysis was performed by one-way or two-way ANOVA followed by Tukey's pairwise comparison post hoc test for normally distributed data, or Kruskal-Wallis test followed by Dunn's post hoc test for non-normally distributed data. For comparison of two groups of normally distributed data, Student's t-test assuming a two-tailed distribution were used. All the error bars represent the standard error of the mean (s.e.m.). P-value of < 0.05 considered statistically significant at the 95% confidence level. The number of biological replicates, raw values and statistical analysis for each experiment was indicated in the figure legends. Independent experiments were performed at least in triplicates.

Table 1. Antibodies and primer used in this study.

	Antigen	Host species	Manufacturer	Cat. Number
Antibody	**Neurofilament M**	Rabbit	Merck	AB1987
	Neurofilament (NF-M)	Mouse	DSHB	2H3
	Laminin	Rabbit	Sigma-Aldrich	L9393
	Laminin2α	Rat	Abcam	ab11576
	TurboGFP	Rabbit	ThermoFisher	PA5-22688
	Choline Acetyltransferase	Goat	Sigma-Aldrich	AB144P
	NeuN	Mouse	Merckmillipore	MAB377

	Primer name	Primer sequence
Primer	**Bap1_F**	5'-TGCCAAATCCCCTATGCAGG-3'
	Bap1_R	5'-TTGCTCAACGATCCTGGCTT-3'
	Gzme_F	5'-CTCCTTTGCTCTCCTTCAACTGAG-3'
	Gzme_R	5'- ATCCACAGACTTAACAAACGCC-3'

References

Anders, S., and Huber, W. (2010). Differential expression analysis for sequence count data. Genome Biology *11*.

Barik, A., Li, L., Sathyamurthy, A., Xiong, W.C., and Mei, L. (2016). Schwann cells in neuromuscular junction formation and maintenance. Journal of Neuroscience *36*, 9770–9781.

Baudet, C., Pozas, E., Adameyko, I., Andersson, E., Ericson, J., and Ernfors, P. (2008). Retrograde signaling onto Ret during motor nerve terminal maturation. Journal of Neuroscience *28*, 963–975.

Bentzinger, C.F., Wang, Y.X., von Maltzahn, J., and Rudnicki, M.A. (2013). The emerging biology of muscle stem cells: Implications for cell-based therapies. BioEssays *35*, 231–241.

Besse, A., Astord, S., Marais, T., Roda, M., Giroux, B., Lejeune, F.X., Relaix, F., Smeriglio, P., Barkats, M., and Biferi, M.G. (2020). AAV9-Mediated Expression of SMN Restricted to Neurons Does Not Rescue the Spinal Muscular Atrophy Phenotype in Mice. Molecular Therapy *28*, 1887–1901.

Boido, M., and Vercelli, A. (2016). Neuromuscular Junctions as Key Contributors and Therapeutic Targets in Spinal Muscular Atrophy. Frontiers in Neuroanatomy *10*, 1–10.

Bononi, A., Giorgi, C., Patergnani, S., Larson, D., Verbruggen, K., Tanji, M., Pellegrini, L., Signorato, V., Olivetto, F., Pastorino, S., et al. (2017). BAP1 regulates IP3R3-mediated Ca 2+ flux to mitochondria suppressing cell transformation. Nature *546*, 549–553.

Bots, M., and Medema, J.P. (2006). Granzymes at a glance. Journal of Cell Science *119*, 5011–5014.

Bowerman, M., Shafey, D., and Kothary, R. (2007). Smn depletion alters profilin II expression and leads to upregulation of the RhoA/ROCK pathway and defects in neuronal integrity. Journal of Molecular Neuroscience *32*, 120–131.

Bowerman, M., Anderson, C.L., Beauvais, A., Boyl, P.P., Witke, W., and Kothary, R. (2009). SMN, profilin IIa and plastin 3: A link between the deregulation of actin dynamics and SMA pathogenesis. Molecular and Cellular Neuroscience *42*, 66–74.

Campanari, M.L., García-Ayllón, M.S., Ciura, S., Sáez-Valero, J., and Kabashi, E. (2016). Neuromuscular junction impairment in amyotrophic lateral sclerosis: Reassessing the role of acetylcholinesterase. Frontiers in Molecular Neuroscience *9*.

Cappellari, O., and Cossu, G. (2013). Pericytes in development and pathology of skeletal muscle. Circulation Research *113*, 341–347.

Catalfamo, M., and Henkart, P.A. (2003). Perforin and the granule exocytosis cytotoxicity pathway. Current Opinion in Immunology *15*, 522–527.

Chae, S., Ahn, B.Y., Byun, K., Cho, Y.M., Yu, M.-H., Lee, B., Hwang, D., Kyong, †, and Park, S. (2013). A Systems Approach for Decoding Mitochondrial Retrograde Signaling Pathways

Chowdhury, D., Beresford, P.J., Zhu, P., Zhang, D., Sung, J.S., Demple, B., Perrino, F.W., and Lieberman, J. (2006). The Exonuclease TREX1 Is in the SET Complex and Acts in Concert with NM23-H1 to Degrade DNA during Granzyme A-Mediated Cell Death. Molecular

Cell *23*, 133–142.

Contreras, O., Cruz–Soca, M., Theret, M., Soliman, H., Tung, L.W., Groppa, E., Rossi, F.M., and Brandan, E. (2019). Cross–talk between TGF–β and PDGFRα signaling pathways regulates the fate of stromal fibro–adipogenic progenitors. J Cell Sci *132*.

DeChiara, T.M., Bowen, D.C., Valenzuela, D.M., Simmons, M. v., Poueymirou, W.T., Thomas, S., Kinetz, E., Compton, D.L., Rojas, E., Park, J.S., et al. (1996). The receptor tyrosine kinase MuSK is required for neuromuscular junction formation in vivo. Cell *85*, 501–512.

Dobin, A., Davis, C.A., Schlesinger, F., Drenkow, J., Zaleski, C., Jha, S., Batut, P., Chaisson, M., and Gingeras, T.R. (2013). STAR: Ultrafast universal RNA–seq aligner. Bioinformatics *29*, 15–21.

Feng, Z., and Ko, C.P. (2008). Schwann cells promote synaptogenesis at the neuromuscular junction via transforming growth factor–β1. Journal of Neuroscience *28*, 9599–9609.

Fox, M.A., Sanes, J.R., Borza, D.B., Eswarakumar, V.P., Fässler, R., Hudson, B.G., John, S.W.M., Ninomiya, Y., Pedchenko, V., Pfaff, S.L., et al. (2007). Distinct Target–Derived Signals Organize Formation, Maturation, and Maintenance of Motor Nerve Terminals. Cell *129*, 179–193.

Frontera, W.R., and Ochala, J. (2015). Skeletal Muscle: A Brief Review of Structure and Function. Behavior Genetics *45*, 183–195.

Gautam, M., Noakes, P.G., Moscoso, L., Rupp, F., Scheller, R.H., Merlie, J.P., and Sanes, J.R. (1996). Defective neuromuscular synaptogenesis in agrin–deficient mutant mice. Cell *85*, 525–535.

Gesemann, M., Denzer, A.J., and Ruegg, M.A. (1995). Acetylcholine receptor-aggregating activity of agrin isoforms and mapping of the active site. Journal of Cell Biology *128*, 625-636.

Giordani, L., He, G.J., Negroni, E., Sakai, H., Law, J.Y.C., Siu, M.M., Wan, R., Corneau, A., Tajbakhsh, S., Cheung, T.H., et al. (2019). High-Dimensional Single-Cell Cartography Reveals Novel Skeletal Muscle-Resident Cell Populations. Molecular Cell *74*, 609-621.e6.

Gonzalez, D., Contreras, O., Rebolledo, D.L., Espinoza, J.P., van Zundert, B., and Brandan, E. (2017). ALS skeletal muscle shows enhanced TGF-β signaling, fibrosis and induction of fibro/adipogenic progenitor markers. PLoS ONE *12*, 1-18.

Granville, D.J. (2010). Granzymes in disease: Bench to bedside. Cell Death and Differentiation *17*, 565-566.

Gromova, A., Tierney, M.T., and Sacco, A. FACS-based Satellite Cell Isolation From Mouse Hind Limb Muscles Materials and Reagents

Grossman, W.J., Revell, P.A., Lu, Z.H., Johnson, H., Bredemeyer, A.J., and Ley, T.J. (2003). The orphan granzymes of humans and mice. Current Opinion in Immunology *15*, 544-552.

Harding, B.N., Kariya, S., Monani, U.R., Chung, W.K., Benton, M., Yum, S.W., Tennekoon, G., and Finkel, R.S. (2015). Spectrum of neuropathophysiology in spinal muscular atrophy type i. Journal of Neuropathology and Experimental Neurology *74*, 15-24.

Hayworth, C.R., Moody, S.E., Chodosh, L.A., Krieg, P., Rimer, M., and Thompson, W.J. (2006). Induction of neuregulin signaling in mouse Schwann cells in vivo mimics responses to denervation. Journal of Neuroscience *26*, 6873-6884.

Henriquez, J.P., Webb, A., Bence, M., Bildsoe, H., Sahores, M., Hughes, S.M., and Salinas, P.C. (2008). Wnt signaling promotes AChR aggregation at the neuromuscular synapse in collaboration with agrin. Proc Natl Acad Sci U S A *105*, 18812-18817.

Heredia, J.E., Mukundan, L., Chen, F.M., Mueller, A.A., Deo, R.C., Locksley, R.M., Rando, T.A., and Chawla, A. (2013). Type 2 innate signals stimulate fibro/adipogenic progenitors to facilitate muscle regeneration. Cell *153*, 376-388.

Hiroyasu, S., Zeglinski, M.R., Zhao, H., Pawluk, M.A., Turner, C.T., Kasprick, A., Tateishi, C., Nishie, W., Burleigh, A., Lennox, P.A., et al. (2021). Granzyme B inhibition reduces disease severity in autoimmune blistering diseases. Nature Communications *12*.

Hua, Y., Sahashi, K., Rigo, F., Hung, G., Horev, G., Bennett, C.F., and Krainer, A.R. (2011). Peripheral SMN restoration is essential for long-term rescue of a severe spinal muscular atrophy mouse model. Nature *478*, 123-126.

Hua, Y., Liu, Y.H., Sahashi, K., Rigo, F., Frank Bennett, C., and Krainer, A.R. (2015). Motor neuron cell-nonautonomous rescue of spinal muscular atrophy phenotypes in mild and severe transgenic mouse models. Genes and Development *29*, 288-297.

Hwang, D., Rust, A.G., Ramsey, S., Smith, J.J., Leslie, D.M., Weston, A.D., de Atauri, P., Aitchison, J.D., Hood, L., Siegel, A.F., et al. (2005). A data integration methodology for systems biology

Jensen, D.E., Proctor, M., Marquis, S.T., Perry Gardner, H., Ha, S.I., Chodosh, L.A., Ishov, A.M., Tommerup, N., Vissing, H., Sekido, Y., et al. (1998). BAP1: a novel ubiquitin hydrolase which binds to the

BRCA1 RING ®nger and enhances BRCA1−mediated cell growth suppression

Jing, L., Lefebvre, J.L., Gordon, L.R., and Granato, M. (2009). Wnt Signals Organize Synaptic Prepattern and Axon Guidance through the Zebrafish unplugged/MuSK Receptor. Neuron *61*, 721–733.

Joe, A.W.B., Yi, L., Natarajan, A., le Grand, F., So, L., Wang, J., Rudnicki, M.A., and Rossi, F.M.V. (2010). Muscle injury activates resident fibro/adipogenic progenitors that facilitate myogenesis. Nature Cell Biology *12*, 153–163.

Johnson, H., Scorrano, L., Korsmeyer, S.J., and Ley, T.J. (2003). Cell death induced by granzyme C. Blood *101*, 3093–3101.

Joshua R. Sanes, and Jeff W. Lichtman (2001). INDUCTION, ASSEMBLY, MATURATION AND MAINTENANCEOF A POSTSYNAPTIC APPARATUS. Nature Reviews Neuroscience *2*, 791–805.

Kang, M., Kim, S., Kim, H., Song, Y., Jung, D., Kang, S., Seo, J.H., Nam, S., and Lee, Y. (2019). Calcium−Binding Polymer−Coated Poly(lactide−co−glycolide) Microparticles for Sustained Release of Quorum Sensing Inhibitors to Prevent Biofilm Formation on Hydroxyapatite Surfaces. ACS Applied Materials and Interfaces *11*, 7686–7694.

Kardon, G., Harfe, B.D., and Tabin, C.J. (2003). A Tcf4−positive mesodermal population provides a prepattern for vertebrate limb muscle patterning. Developmental Cell *5*, 937–944.

Kariya, S., Park, G.H., Maeno−Hikichi, Y., Leykekhman, O., Lutz, C., Arkovitz, M.S., Landmesser, L.T., and Monani, U.R. (2008). Reduced

SMN protein impairs maturation of the neuromuscular junctions in mouse models of spinal muscular atrophy. Human Molecular Genetics *17*, 2552–2569.

Kariya, S., Obis, T., Garone, C., Akay, T., Sera, F., Iwata, S., Homma, S., and Monani, U.R. (2014). Requirement of enhanced Survival Motoneuron protein imposed during neuromuscular junction maturation. Journal of Clinical Investigation *124*, 785–800.

Kelly, J.M., Waterhouse, N.J., Cretney, E., Browne, K.A., Ellis, S., Trapani, J.A., and Smyth, M.J. (2004). Granzyme M mediates a novel form of perforin-dependent cell death. Journal of Biological Chemistry *279*, 22236–22242.

Kim, J.H., Kang, J.S., Yoo, K., Jeong, J., Park, I., Park, J.H., Rhee, J., Jeon, S., Jo, Y.W., Hann, S.H., et al. (2022). Bap1/SMN axis in Dpp4+ skeletal muscle mesenchymal cells regulates the neuromuscular system. JCI Insight *7*.

Kim, K.E., Park, I., Kim, J., Kang, M.G., Choi, W.G., Shin, H., Kim, J.S., Rhee, H.W., and Suh, J.M. (2021). Dynamic tracking and identification of tissue-specific secretory proteins in the circulation of live mice. Nature Communications *12*.

Kreutzer, M., Seehusen, F., Kreutzer, R., Pringproa, K., Kummerfeld, M., Claus, P., Deschl, U., Kalkul, A., Beineke, A., Baumgärtner, W., et al. (2012). Axonopathy is associated with complex axonal transport defects in a model of multiple sclerosis. Brain Pathology *22*, 454–471.

Lemos, D.R., Babaeijandaghi, F., Low, M., Chang, C.K., Lee, S.T., Fiore, D., Zhang, R.H., Natarajan, A., Nedospasov, S.A., and Rossi, F.M.V. (2015). Nilotinib reduces muscle fibrosis in chronic muscle

injury by promoting TNF-mediated apoptosis of fibro/adipogenic progenitors. Nature Medicine *21*, 786-794.

Li, J., Ito, M., Ohkawara, B., Masuda, A., and Ohno, K. (2018). Differential effects of spinal motor neuron-derived and skeletal muscle-derived Rspo2 on acetylcholine receptor clustering at the neuromuscular junction. Scientific Reports *8*, 1-14.

Lin, W., Sanchez, H.B., Deerinck, T., Morris, J.K., Ellisman, M., and Lee, K.-F. (2000). Aberrant development of motor axons and neuromuscular synapses in erbB2-deficient mice. PNAS *97*, 1299-1304.

Lin, W., Burgess, R.W., Dominguez, B., Pfaff, S.L., Sanes, J.R., and Lee, K.F. (2001). Distinct roles of nerve and muscle in postsynaptic differentiation of the neuromuscular synapse. Nature *410*, 1057-1064.

Louie, B.H., and Kurzrock, R. (2020). BAP1: Not just a BRCA1-associated protein. Cancer Treatment Reviews *90*.

Lukjanenko, L., Karaz, S., Stuelsatz, P., Gurriaran-Rodriguez, U., Michaud, J., Dammone, G., Sizzano, F., Mashinchian, O., Ancel, S., Migliavacca, E., et al. (2019). Aging Disrupts Muscle Stem Cell Function by Impairing Matricellular WISP1 Secretion from Fibro-Adipogenic Progenitors. Cell Stem Cell *24*, 433-446.e7.

Machida, Y.J., Machida, Y., Vashisht, A.A., Wohlschlegel, J.A., and Dutta, A. (2009). The deubiquitinating enzyme BAP1 regulates cell growth via interaction with HCF-1. Journal of Biological Chemistry *284*, 34179-34188.

Madaro, L., Passafaro, M., Sala, D., Etxaniz, U., Lugarini, F., Proietti,

D., Alfonsi, M.V., Nicoletti, C., Gatto, S., de Bardi, M., et al. (2018). Denervation-activated STAT3-IL-6 signalling in fibro-adipogenic progenitors promotes myofibres atrophy and fibrosis. Nature Cell Biology *20*, 917-927.

Malecova, B., Gatto, S., Etxaniz, U., Passafaro, M., Cortez, A., Nicoletti, C., Giordani, L., Torcinaro, A., de Bardi, M., Bicciato, S., et al. (2018). Dynamics of cellular states of fibro-adipogenic progenitors during myogenesis and muscular dystrophy. Nature Communications *9*, 3670.

Mark S. Pasternack, and Herman N. Eisen (1985). A novel serine esterase expressed by cytotoxic T lymphocytes. Nature *314*, 743-745.

Martinvalet, D., Zhu, P., and Lieberman, J. (2005). Granzyme A induces caspase-independent mitochondrial damage, a required first step for apoptosis. Immunity *22*, 355-370.

Mathew, S.J., Hansen, J.M., Merrell, A.J., Murphy, M.M., Lawson, J.A., Hutcheson, D.A., Hansen, M.S., Angus-Hill, M., and Kardon, G. (2011). Connective tissue fibroblasts and Tcf4 regulate myogenesis. Development *138*, 371-384.

McCabe, B.D., Hom, S., Aberle, H., Fetter, R.D., Marques, G., Haerry, T.E., Wan, H., O' Connor, M.B., Goodman, C.S., and Haghighi, A.P. (2004). Highwire regulates presynaptic BMP signaling essential for synaptic growth. Neuron *41*, 891-905.

McGovern, V.L., Iyer, C.C., David Arnold, W., Gombash, S.E., Zaworski, P.G., Blatnik, A.J., Foust, K.D., and Burghes, A.H.M. (2015). SMN expression is required in motor neurons to rescue

electrophysiological deficits in the SMN⊿7 mouse model of SMA. Human Molecular Genetics *24*, 5524–5541.

Moloney, E.B., de Winter, F., and Verhaagen, J. (2014). ALS as a distal axonopathy: Molecular mechanisms affecting neuromuscular junction stability in the presymptomatic stages of the disease. Frontiers in Neuroscience *8*, 1–18.

Mozzetta, C., Consalvi, S., Saccone, V., Tierney, M., Diamantini, A., Mitchell, K.J., Marazzi, G., Borsellino, G., Battistini, L., Sassoon, D., et al. (2013). Fibroadipogenic progenitors mediate the ability of HDAC inhibitors to promote regeneration in dystrophic muscles of young, but not old Mdx mice. EMBO Molecular Medicine *5*, 626–639.

Mukhamedshina, Y., Gracheva, O., Mukhutdinova, D., Chelyshev, Y., and Rizvanov, A. (2019). Mesenchymal stem cells and the neuronal microenvironment in the area of spinal cord injury. Neural Regeneration Research *14*, 227–237.

Mukund, K., and Subramaniam, S. (2020). Skeletal muscle: A review of molecular structure and function, in health and disease. Wiley Interdisciplinary Reviews: Systems Biology and Medicine *12*.

Murali, R., Wiesner, T., and Scolyer, R.A. (2013). Tumours associated with BAP1 mutations. Pathology *45*, 116–126.

Nishikawa, H., Wu, W., Koike, A., Kojima, R., Gomi, H., Fukuda, M., and Ohta, T. (2009). BRCA1−associated protein 1 interferes with BRCA1/BARD1 RING heterodimer activity. Cancer Research *69*, 111–119.

Nishimune, H., Valdez, G., Jarad, G., Moulson, C.L., Müller, U., Miner, J.H., and Sanes, J.R. (2008). Laminins promote postsynaptic

maturation by an autocrine mechanism at the neuromuscular junction. Journal of Cell Biology *182*, 1201–1215.

Oprescu, S.N., Yue, F., Qiu, J., Brito, L.F., and Kuang, S. (2020). Temporal Dynamics and Heterogeneity of Cell Populations during Skeletal Muscle Regeneration. IScience *23*, 100993.

Pillon, N.J., Bilan, P.J., Fink, L.N., and Klip, A. (2013). Cross-talk between skeletal muscle and immune cells: muscle-derived mediators and metabolic implications. Am J Physiol Endocrinol Metab *304*, 453–465.

Pollari, E., Goldsteins, G., Bart, G., Koistinaho, J., and Giniatullin, R. (2014). The role of oxidative stress in degeneration of the neuromuscular junction in amyotrophic lateral sclerosis. Frontiers in Cellular Neuroscience *8*, 1–8.

Pollari, E., Prior, R., Robberecht, W., van Damme, P., and van den Bosch, L. (2018). In vivo electrophysiological measurement of compound muscle action potential from the forelimbs in mouse models of motor neuron degeneration. Journal of Visualized Experiments *2018*.

Relaix, F., Bencze, M., Borok, M.J., der Vartanian, A., Gattazzo, F., Mademtzoglou, D., Perez-Diaz, S., Prola, A., Reyes-Fernandez, P.C., Rotini, A., et al. (2021). Perspectives on skeletal muscle stem cells. Nature Communications *12*.

Remédio, L., Gribble, K.D., Lee, J.K., Kim, N., Hallock, P.T., Delestrée, N., Mentis, G.Z., Froemke, R.C., Granato, M., and Burden, S.J. (2016). Diverging roles for Lrp4 and wnt signaling in neuromuscular synapse development during evolution. Genes and Development *30*, 1058–

1069.

Rodríguez Cruz, P.M., Cossins, J., Beeson, D., and Vincent, A. (2020). The Neuromuscular Junction in Health and Disease: Molecular Mechanisms Governing Synaptic Formation and Homeostasis. Frontiers in Molecular Neuroscience *13*.

Rönnberg, E., Calounova, G., Guss, B., Lundequist, A., and Pejler, G. (2013). Granzyme D is a novel murine mast cell protease that is highly induced by multiple pathways of mast cell activation. Infection and Immunity *81*, 2085-2094.

Ryan, J.M., Barry, F.P., Murphy, J.M., and Mahon, B.P. (2005). Mesenchymal stem cells avoid allogeneic rejection. Journal of Inflammation *2*, 1-11.

Saito, Y., Chikenji, T.S., Matsumura, T., Nakano, M., and Fujimiya, M. (2020). Exercise enhances skeletal muscle regeneration by promoting senescence in fibro-adipogenic progenitors. Nature Communications *11*.

Scheuermann, J.C., de Ayala Alonso, A.G., Oktaba, K., Ly-Hartig, N., McGinty, R.K., Fraterman, S., Wilm, M., Muir, T.W., and Müller, J. (2010). Histone H2A deubiquitinase activity of the Polycomb repressive complex PR-DUB. Nature *465*, 243-247.

Schmidt, N., Akaaboune, M., Gajendran, N., Martinez-Pena y Valenzuela, I., Wakefield, S., Thurnheer, R., and Brenner, H.R. (2011). Neuregulin/ErbB regulate neuromuscular junction development by phosphorylation of α-dystrobrevin. Journal of Cell Biology *195*, 1171-1184.

Sciorati, C., Rigamonti, E., Manfredi, A.A., and Rovere-Querini, P.

(2016). Cell death, clearance and immunity in the skeletal muscle. Cell Death and Differentiation *23*, 927–937.

Scott, R.W., Arostegui, M., Schweitzer, R., Rossi, F.M.V., and Underhill, T.M. (2019). Hic1 Defines Quiescent Mesenchymal Progenitor Subpopulations with Distinct Functions and Fates in Skeletal Muscle Regeneration. Cell Stem Cell *25*, 797–813.e9.

Shi, L., Wu, L., Wang, S., and Fan, Z. (2009). Granzyme F induces a novel death pathway characterized by Bid–independent cytochrome c release without caspase activation. Cell Death and Differentiation *16*, 1694–1706.

Shi, L., Fu, A.K.Y., and Ip, N.Y. (2012). Molecular mechanisms underlying maturation and maintenance of the vertebrate neuromuscular junction. Trends in Neurosciences *35*, 441–453.

Shrestha, R., Nabavi, N., Lin, Y.Y., Mo, F., Anderson, S., Volik, S., Adomat, H.H., Lin, D., Xue, H., Dong, X., et al. (2019). BAP1 haploinsufficiency predicts a distinct immunogenic class of malignant peritoneal mesothelioma. Genome Medicine *11*.

Stanga, S., Boido, M., and Kienlen–Campard, P. (2021). How to build and to protect the neuromuscular junction: The role of the glial cell line–derived neurotrophic factor. International Journal of Molecular Sciences *22*, 1–14.

Tezuka, T., Inoue, A., Hoshi, T., Weatherbee, S.D., Burgess, R.W., Ueta, R., and Yamanashi, Y. (2014). The MuSK activator agrin has a separate role essential for postnatal maintenance of neuromuscular synapses. Proc Natl Acad Sci U S A *111*, 16556–16561.

Theret, M., Rossi, F.M.V., and Contreras, O. (2021). Evolving Roles

of Muscle-Resident Fibro-Adipogenic Progenitors in Health, Regeneration, Neuromuscular Disorders, and Aging. Frontiers in Physiology *12*.

Trapani, J.A., and Sutton, V.R. (2003). Granzyme B: Pro-apoptotic, antiviral and antitumor functions. Current Opinion in Immunology *15*, 533-543.

Tsai, T.-C., Lin, W., Yang, S.-H., Cheong, W.T., Cheng, E.-H., Lee, M.-S., Chong, K.-Y., and Chen, C.-M. (2010). Granzyme G is expressed in the two-cell stage mouse embryo and is required for the maternal-zygotic transition. BMC Developmental Biology *10*.

Uezumi, A., Fukada, S.I., Yamamoto, N., Takeda, S., and Tsuchida, K. (2010). Mesenchymal progenitors distinct from satellite cells contribute to ectopic fat cell formation in skeletal muscle. Nature Cell Biology *12*, 143-152.

Uezumi, A., Ito, T., Morikawa, D., Shimizu, N., Yoneda, T., Segawa, M., Yamaguchi, M., Ogawa, R., Matev, M.M., Miyagoe-Suzuki, Y., et al. (2011). Fibrosis and adipogenesis originate from a common mesenchymal progenitor in skeletal muscle. Journal of Cell Science *124*, 3654-3664.

Uezumi, A., Ikemoto-Uezumi, M., and Tsuchida, K. (2014). Roles of nonmyogenic mesenchymal progenitors in pathogenesis and regeneration of skeletal muscle. Frontiers in Physiology *5 FEB*, 1-11.

Uezumi, A., Ikemoto-Uezumi, M., Zhou, H., Kurosawa, T., Yoshimoto, Y., Nakatani, M., Hitachi, K., Yamaguchi, H., Wakatsuki, S., Araki, T., et al. (2021). Mesenchymal Bmp3b expression maintains skeletal muscle integrity and decreases in age-related sarcopenia. Journal of

Clinical Investigation *131*.

Valsecchi, V., Boido, M., de Amicis, E., Piras, A., and Vercelli, A. (2015). Expression of muscle-specific MiRNA 206 in the progression of disease in a murine SMA model. PLoS ONE *10*, 1-17.

Ventii, K.H., Devi, N.S., Friedrich, K.L., Chernova, T.A., Tighiouart, M., van Meir, E.G., and Wilkinson, K.D. (2008). BRCA1-associated protein-1 is a tumor suppressor that requires deubiquitinating activity and nuclear localization. Cancer Research *68*, 6953-6962.

Voskoboinik, I., Whisstock, J.C., and Trapani, J.A. (2015). Perforin and granzymes: Function, dysfunction and human pathology. Nature Reviews Immunology *15*, 388-400.

Wang, A., Papneja, A., Hyrcza, M., Al-Habeeb, A., and Ghazarian, D. (2016). BAP1: Gene of the month. Journal of Clinical Pathology *69*, 750-753.

Wosczyna, M.N., Konishi, C.T., Perez Carbajal, E.E., Wang, T.T., Walsh, R.A., Gan, Q., Wagner, M.W., and Rando, T.A. (2019). Mesenchymal Stromal Cells Are Required for Regeneration and Homeostatic Maintenance of Skeletal Muscle. Cell Reports *27*, 2029-2035.e5.

Wu, H., Xiong, W.C., and Mei, L. (2010). To build a synapse: Signaling pathways in neuromuscular junction assembly. Development *137*, 1017-1033.

Wyatt, T.J., and Keirstead, H.S. (2010). Stem cell-derived neurotrophic support for the neuromuscular junction in spinal muscular atrophy. Expert Opinion on Biological Therapy *10*, 1587-1594.

Yang, J.F., Cao, G., Koirala, S., Reddy, L. v., and Ko, C.P. (2001). Schwann cells express active agrin and enhance aggregation of acetylcholine receptors on muscle fibers. Journal of Neuroscience *21*, 9572–9584.

Zhao, W., Steinfeld, J.B., Liang, F., Chen, X., Maranon, D.G., Jian Ma, C., Kwon, Y., Rao, T., Wang, W., Sheng, C., et al. (2017). BRCA1–BARD1 promotes RAD51–mediated homologous DNA pairing. Nature *550*.

국 문 초 록

근육은 인체 질량의 절반 가까이를 차지하는 조직으로 근섬유세포, 근육 줄기세포, 운동 신경, 섬유-지방성 전구세포 등 다양한 세포의 기능으로 유지된다. 근육의 섬유-지방성 전구세포는 근육 조직 내에 존재하는 간충직 세포로 근육의 항상성을 유지하고 근육 손상 이후 근육 재생 과정과 근육 줄기세포의 활성을 조절하는 것으로 알려져 있다. 그러나 섬유-지방성 전구세포가 근육의 다른 세포들과 어떤 상호작용을 하는지는 잘 알려져 있지 않다.

신경-근육접합은 근육과 운동신경 사이에 존재하는 시냅스로 운동신경의 전기적 신호가 아세틸콜린의 화학 신호로 전환되어 근육의 수축 유도가 발생하는 곳이다. 근육의 적절한 기능을 위해서는 신경-근육접합의 통합적이고 조절된 신호가 매우 중요하다. 이에 따라 신경-근육접합의 구조와 기능의 형성과 성숙, 유지를 조절하는 아그린, 뉴레귤린, 아세틸콜린 등의 신호와 이들이 어떻게 작동하는지에 관한 연구가 많이 진행되었다. 하지만 온몸의 신경-근육접합이 어떻게 전체적으로 비슷한 양상으로 조절되는지에 대해서는 잘 알려지지 않았다. 본 연구에서는 근육의 섬유-지방성 전구세포가 온몸의 운동 신경이 살아남고 신경-근육접합이 성숙하고 유지되도록 하는데 중요한 역할을 하는 것을 밝혔다. 신경-근육접합에 문제가 있는 마우스 모델의 근육 조직에 국소적 섬유-지방성 전구세포 투여를 통해 온몸의 신경-근육접합이 정상화되는 것을 확인하였고 이를 통해 섬유-지방성 전구세포가 신경-근육접합의 발달에 필요함을 확인하였다. 섬유-지방성 전구세포의 전사체와 분비체를 분석하여 granzyme E라는 단백질을

새로이 밝혔고 섬유-지방성 전구세포에서 특이적으로 본 단백질을 발현, 분비하여 신경-근육접합과 운동 신경을 조절함을 확인하였다. 본 연구는 신경과의 연결을 통해 근육의 기능을 유지하는 새로운 메커니즘을 제시했으며 신경과 근육 및 섬유-지방성 전구세포와의 관계에 대한 통합적인 이해를 제공한다.

주요어 : 근육 간충직세포; 섬유-지방성 전구세포; 신경근육접합; Granzyme

학 번 : 2015-20431